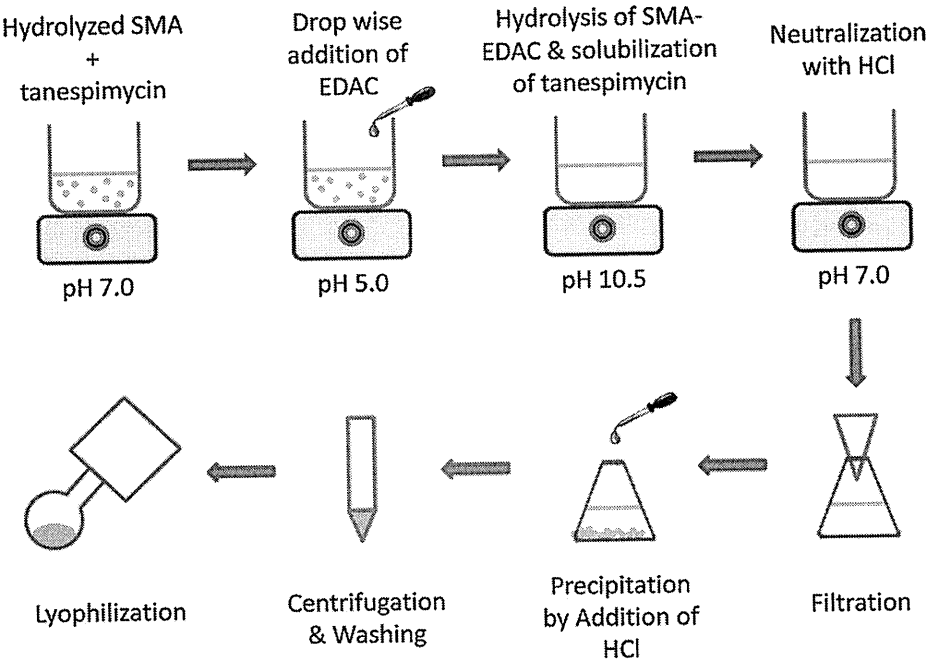

Fig. 1. Preparation of SMA-tanespimycin micelles. SMA-tanespimycin micelles were prepared by first suspending tanespimycin in an aqueous solution of hydrolyzed SMA containing EDAC. The solution was then adjusted to alkaline conditions which resulted in encapsulation of tanespimycin by SMA micelles. The resulting solution was neutralized and SMA-tanespimycin micelles isolated.

The ability of SMA based micelles to achieve high drug loading has previously been demonstrated for the hydrophobic drugs zinc protoporphyrin (Iyer et al., 2007) and doxorubicin (Greish et al., 2004). In the current study, a high drug loading of 25.6% tanespimycin by weight was observed for SMA-tanespimycin as determined by UV spectrophotometry (Table 1). The micelles were highly soluble, with a drug equivalent aqueous solubility of >5.0 mg/mL as measured in pH 7.4 PBS buffer, whereas free tanespimycin was soluble only at 0.021 mg/mL. To ensure that tanespimycin remained unmodified during micelle preparation, SMA-tanespimycin in comparison with free tanespimycin was analyzed by RP-HPLC. Both tanespimycin and SMA-tanespimycin showed a prominent peak at 15.2 min, and both peaks exhibited UV spectra characteristic of tanespimycin (data not shown). Drug loading of tanespimycin as determined by RP-HPLC was 25.2% by weight and in agreement with drug loading determined by UV spectrophotometry.

Size is a critical parameter for macromolecular drug delivery systems designed to escape renal filtration. It has been proposed that carriers with sizes greater than 10 nm accumulate in the tumor tissues via the EPR effect. SMA-tanespimycin micelles had a mean diameter of 74 ± 7 nm and a polydispersity index of 0.31 ± 0.08 as measured by dynamic light scattering (Fig. 2). The micelles had a zeta potential of -35 ± 3 mV as measured in a 50 mM phosphate buffer at pH 7.4. SMA micelles were characterized by carboxyl terminated maleic acid surface groups which impart a negative charge to the micelles.

The high loading efficiency and possibility to tune the loading ratio of tanespimycin into SMA micelles represents significant advantages for industrial scale up, in contrast to many other micellar systems.

Table 1
Characteristics of SMA-tanespimycin micelles.

Property	Mean	SD
Amount of tanespimycin introduced for micelle preparation (mg)	150.0	–
Drug loading efficiency (%)[a]	93.1	–
Drug loading (% wt/wt)	25.6	–
Mean micelle diameter (nm)[b,c]	74	7
Polydispersity index	0.31	0.08
Zeta potential[c](mV)	−35	3

[a] Drug loading efficiency calculated as mg tanespimycin solubilized by SMA micelles/mg tanespimycin introduced for micelle preparation.
[b] Z-Average size as measured by dynamic light scattering (DLS).
[c] As measured in 50 mM phosphate buffer at pH 7.4.

3.3. Release of tanespimycin from SMA-tanespimycin micelles

The incorporation of tanespimycin into SMA micelles can increase tumor uptake and alter biodistribution, resulting in an increase in the therapeutic index of the drug. For this to occur, it is essential that tanespimycin is retained by the carrier for a period of time to allow drug accumulation in tumor tissue via

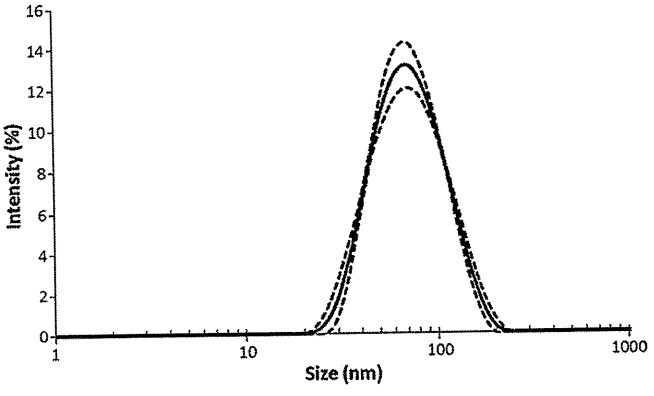

Fig. 2. Size distribution of SMA-tanespimycin micelles. The size distribution of SMA-tanespimycin micelles was determined using a Malvern Zeta Sizer at a concentration of 1.0 mg/mL at pH 7.4. Data are expressed as mean (solid line) ± SD (dashed line) ($N = 3$).

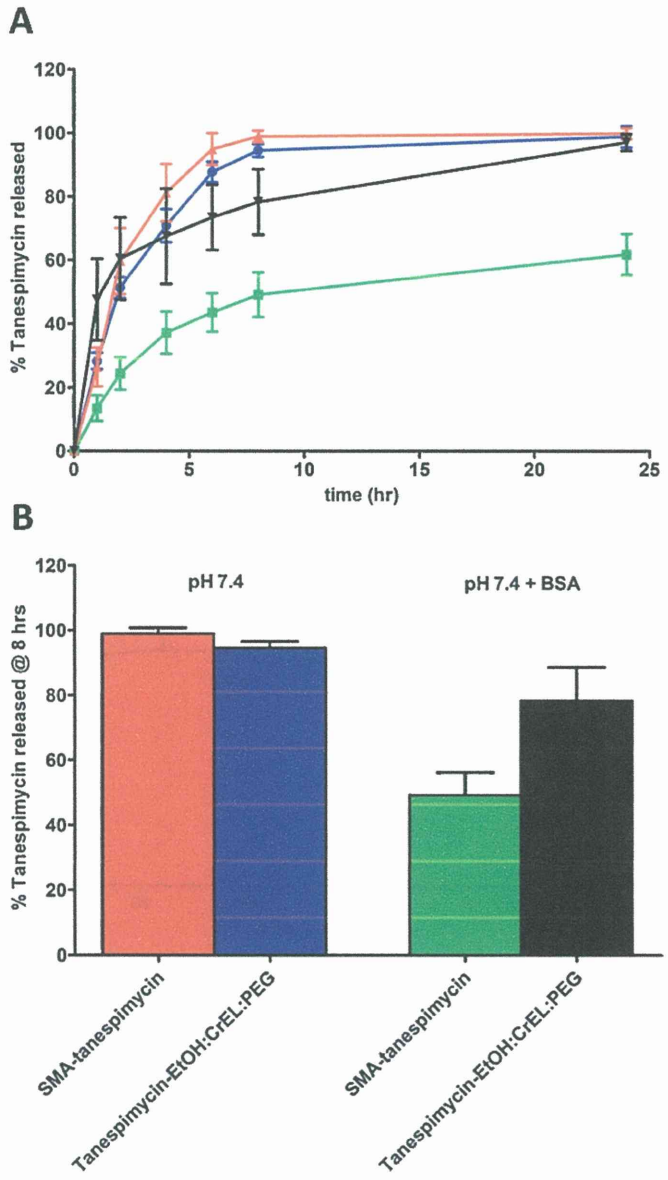

Fig. 3. Release of tanespimycin from SMA-tanespimycin. Release of tanespimycin from SMA micelles was evaluated using a dialysis method and compared to tanespimycin formulated in EtOH:CrEL:PEG as control. (A) Release of tanespimycin from SMA-tanespimycin (red) and tanespimycin-EtOH:CrEL:PEG (blue) in a pH 7.4 buffer and release of tanespimycin from SMA-tanespimycin (green) and tanespimycin-EtOH:CrEL:PEG (black) in a pH 7.4 buffer containing 40 mg/mL BSA. (B) Release of tanespimycin at 8 h. Data expressed as mean ± SD ($N = 3$). *Difference detected at $p < 0.05$ significance level. (For interpretation of the references to color in the figure caption, the reader is referred to the web version of the article.)

the EPR effect. However, release from the carrier is also essential to allow tanespimycin to elicit its pharmacologic effect. Release rate is therefore a critical parameter in anticancer macromolecular drug delivery, and an ideal anticancer carrier should be able to retain its cargo for approximately 6 h while tumor accumulation occurs (Greish, 2007), followed by complete drug release. To address this issue, the *in vitro* release rate of tanespimycin from SMA-tanespimycin micelles was evaluated using a dialysis method and compared to the release of tanespimycin formulated in EtOH:CrEL:PEG. Release was assessed in a pH 7.4 buffer where 51% and 95% tanespimycin was released from SMA-tanespimycin micelles in 2 and 8 h, respectively. Release from tanespimycin formulated in EtOH:CrEL:PEG was not significantly different, with 60% and 99% released in 2 and 8 h, respectively. To better ascertain release of tanespimycin from the blood plasma compartment *in vivo*, a second test condition was evaluated wherein BSA was included inside the dialysis bag at a physiologically relevant concentration of 40 mg/mL. Release of tanespimycin from SMA-tanespimycin micelles in the presence of BSA was reduced at all time points greater that 1 h ($p < 0.001$) as compared to release from pH 7.4 buffer alone (Fig. 3). Release of tanespimycin from SMA-tanespimycin micelles was also significantly reduced as compared to tanespimycin formulated in EtOH:CrEL:PEG at all time points greater than 1 h ($p < 0.001$), with only 62% release observed in 24 h (Fig. 3). This reduction in release rate can be explained by the well characterized noncovalent binding of SMA to serum albumin (Kobayashi et al., 1988), and it is thus anticipated that serum albumin can serve as a secondary carrier for SMA-tanespimycin micelles *in vivo*.

3.4. Cytotoxicity of SMA-tanespimycin micelles in vitro

The ability of SMA-tanespimycin micelles to inhibit the growth of DU145 human prostate cancer cells was evaluated *in vitro* using a WST-8 cell viability assay. Incorporation of tanespimycin into SMA-tanespimycin micelles resulted in a decrease in its ability to inhibit the growth of DU145 cells with an IC_{50} of 230 ± 10 nM as compared to an IC_{50} of 15.0 ± 0.3 nM for tanespimycin solubilized in EtOH:CrEL:PEG (Fig. 4). For controls, SMA and EtOH:CrEL:PEG solutions were subjected to the same dilution protocol and evaluated for growth inhibition ability and showed no cytotoxicity over an equivalent concentration range. During the 72 h incubation time of these studies, the release of tanespimycin from SMA-tanespimycin micelles was most likely minimized because of the lack of a perpetual sink condition. Although SMA-tanespimycin micelles were less toxic as compared to free tanespimycin, they remained cytotoxic in the nanomolar concentration range. This reduction in cytotoxicity of SMA-tanespimycin micelles as compared to free tanespimycin can be explained by a number of possible factors. The micelles first need to be taken up by cells via endocytosis, whereas tanespimycin can passively diffuse across cellular membranes. Uptake of the micelles could further be reduced due to the interactions of the negatively charged carboxylic acid rich surface of the micelles with negatively charged membranes. Tanespimycin must also be released from the micelle core in order for it to elicit its pharmacological effect, which occurs over a prolonged time interval, further reducing overall cytotoxic exposure. The reduced toxicity of SMA-tanespimycin micelles can potentially be advantageous in an *in vivo* scenario by minimizing systemic exposure of tanespimycin while allowing time for accumulation in tumor tissues to occur.

3.5. In vivo efficacy of SMA-tanespimycin micelles

The delivery of tanespimycin via SMA-tanespimycin micelles results in an increase in the therapeutic index for tanespimycin. Toward this aim, a preliminary *in vivo* efficacy study was performed in athymic nu/nu mice bearing subcutaneous DU145 human prostate cancer xenografts. As accumulation in tumor tissues via the EPR effect was anticipated for SMA-tanespimycin micelles, a subtherapeutic dose of 10 mg/kg tanespimycin equivalent was used. A single dose of SMA-tanespimycin micelles, free tanespimycin, or saline were injected via tail-vein injection and animals were monitored twice weekly for changes in tumor volume as an indicator of efficacy (Fig. 5). Body weight was also recorded as an indicator of general toxicity (Fig. 5). At a single dose of 10 mg/kg tanespimycin equivalent, SMA-tanepsimycin micelles resulted in a reduction in normalized mean tumor volume that was maintained throughout the duration of the study (23 days), whereas

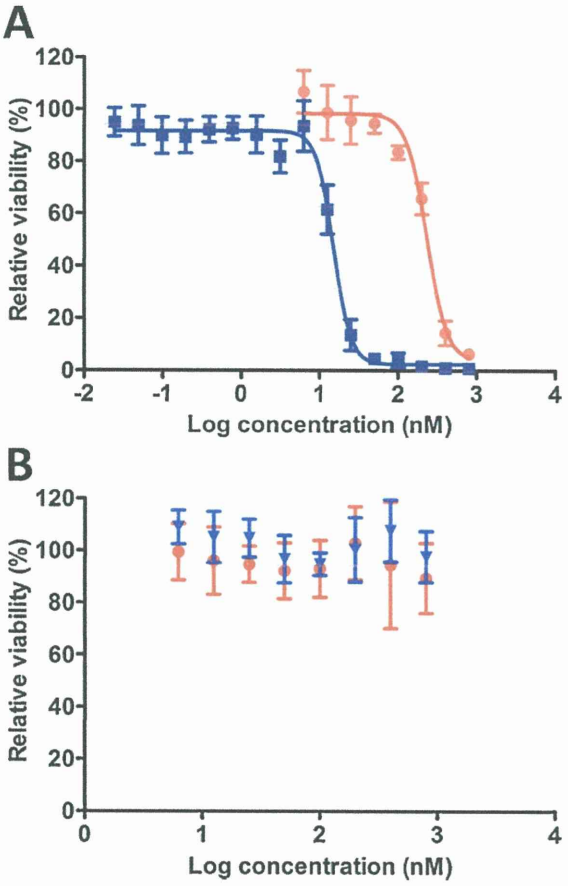

Fig. 4. Cell growth inhibition of SMA-tanespimycin micelles. DU145 human prostate cancer cells were treated for 72 h with increasing drug equivalent concentrations of tanespimycin formulated in EtOH:CrEL:PEG (blue), SMA-tanespimycin micelles (red) (A), EtOH:CreEL:PEG vehicle alone (blue) or hydrolyzed SMA (red) (B). Following treatment, cell viability was assessed by WST-8 assay. Non-linear regression and IC_{50} values were determined by analysis using GraphPad Prism. (For interpretation of the references to color in the figure caption, the reader is referred to the web version of the article.)

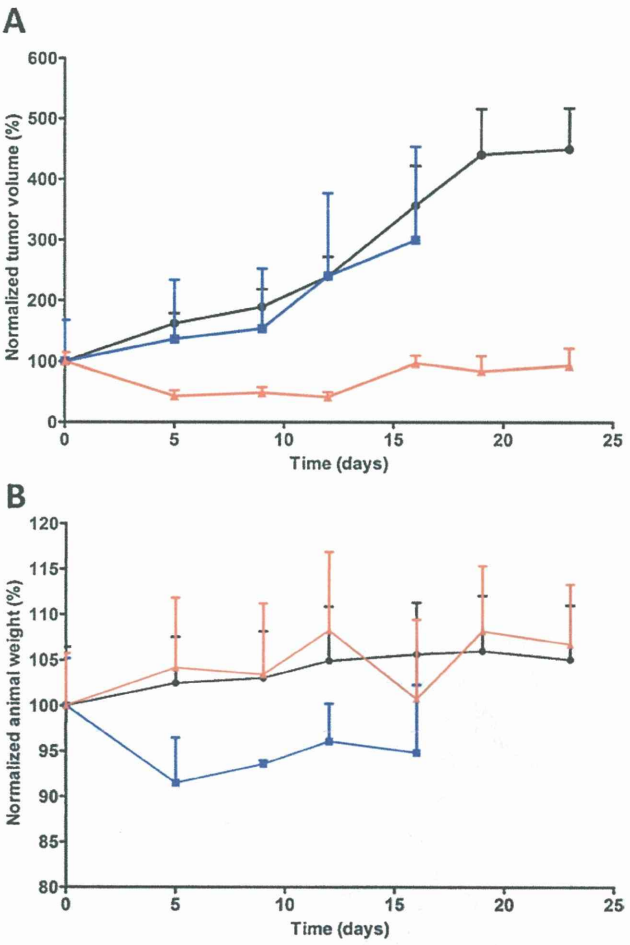

Fig. 5. *In vivo* efficacy of SMA-tanespimycin micelles. Athymic nu/nu mice bearing DU145 tumor xenografts were treated IV with a single dose of 10 mg/kg tanespimycin (blue) or 10 mg/kg tanespimycin equivalent SMA-tanespimycin micelles (red) and compared with a saline injection control group (black). (A) Normalized tumor volume was measured as a function of time for each treatment group. (B) Normalized animal weight was assessed as a measure of general toxicity. Data are expressed as mean ± SEM ($N = 5$ per treatment group). *Difference detected at $p < 0.05$ significance level. (For interpretation of the references to color in the figure caption, the reader is referred to the web version of the article.)

normalized mean tumor volume in saline injected animals increased 450%. Relative to saline injected animals, SMA-tanespimycin resulted in a statistically significant decrease in normalized mean tumor volume at all time points following treatment ($p < 0.05$). A single dose of free tanespimycin showed no evidence of efficacy at 10 mg/kg, and normalized mean tumor volume was not different from saline injected animals at all time points. Animals in the free tanespimycin group were euthanized on day 16 as one animal showed excessive tumor burden. SMA-tanespimycin micelles in comparison with free tanespimycin showed a significant reduction in normalized mean tumor volume on day 16 ($p < 0.05$). These results coupled with the *in vitro* cytotoxicity results suggest that SMA-tanespimycin micelles have the ability to accumulate in tumor tissues and inhibit tumor growth *in vivo*.

Animal weights were measured twice a week as an indicator of general toxicity during the efficacy study. Relative to saline injected animals, animals treated with SMA-tanespimycin micelles showed no difference in normalized mean animal weight during the study. An 11% reduction in normalized mean animal weight was observed for free tanespimycin as compared to saline injected animals at day 5 ($p < 0.05$); differences detected at subsequent time points were not statistically significant. However, it is unclear whether the solvent used to solubilize tanespimycin has contributed to the overt tanespimycin toxicity in this study, or the manifested toxicity was totally due to the free drug. These results demonstrate that SMA-tanespimycin micelles were well tolerated.

This efficacy study was preliminary in its nature as parameters such as maximum tolerated dose and dosing schedule were not optimized. However, the results of the study demonstrate that SMA-tanespimycin micelles were well tolerated and effective in reducing DU145 tumor growth, and suggest that the therapeutic index of tanespimycin is increased by encapsulation in SMA micelles.

Overall, the data from this study demonstrates that delivery of tanespimycin using SMA micelles has several distinct advantages. First, the aqueous solubility of tanespimycin is increased by encapsulation into SMA micelles, and because these interactions are non-covalent, the potent activity of tanespimycin is maintained. Second, the preparation of SMA-tanespimycin micelles is simple, straightforward, and efficient in loading tanespimycin, thus allowing cost efficient scale up at later stages of development. Third, the macromolecular nature of SMA-tanespimycin micelles allows accumulation into tumor tissues, resulting in an increase in the therapeutic index of tanespimycin. These features combine to suggest that SMA-tanespimycin micelles have the potential to increase the efficacy and safety profile of tanespimycin.

4. Conclusion

SMA-tanespimycin micelles were prepared in a simple manner with a high loading drug efficiency of 93%. The micelles incorporated 25.6% tanespimycin by weight and exhibited properties that allow for increased blood circulation and tumor accumulation *in vivo*. Tanespimycin was released from the micelles in a controlled manner and showed potent activity against DU145 human prostate cancer cells *in vitro*. The micelles also were well tolerated and exhibited potent anti-cancer activity in nu/nu mice bearing subcutaneous DU145 human prostate cancer tumor xenografts, with a significant increase in efficacy as measured by tumor regression as compared to free tanespimycin at an equivalent single dose of 10 mg/kg. These data suggest that the therapeutic index of tanespimycin is increased by incorporation into SMA micelles.

Acknowledgements

This research was supported by the National Institutes of Health grant R01 EB007171 and the Utah Science Technology and Research (USTAR) initiative.

References

Banerji, U., O'donnell, A., Scurr, M., Pacey, S., Stapleton, S., Asad, Y., Simmons, L., Maloney, A., Raynaud, F., Campbell, M., Walton, M., Lakhani, S., Kaye, S., Workman, P., Judson, I., 2005. Phase I pharmacokinetic and pharmacodynamic study of 17-allylamino, 17-demethoxygeldanamycin in patients with advanced malignancies. J. Clin. Oncol. 23, 4152–4161.

Blanco, E., Kessinger, C.W., Sumer, B.D., Gao, J., 2009. Multifunctional micellar nanomedicine for cancer therapy. Exp. Biol. Med. 234, 123–131.

Borgman, M.P., Aras, O., Geyser-Stoops, S., Sausville, E.A., Ghandehari, H., 2009. Biodistribution of HPMA copolymer-aminohexylgeldanamycin-RGDfK conjugates for prostate cancer drug delivery. Mol. Pharm. 6, 1836–1847.

Buchner, J., 1999. Hsp90 & Co.—a holding for folding. Trends Biochem. Sci. 24, 136–141.

Burger, A.M., Fiebig, H.H., Stinson, S.F., Sausville, E.A., 2004. 17-(Allylamino)-17-demethoxygeldanamycin activity in human melanoma models. Anticancer Drugs 15, 377–387.

Claracq, J., Santos, S.F.C.R., Duhamel, J., Dumousseaux, C., Corpart, J.-M., 2002. Rigid interior of styrene–maleic anhydride copolymer aggregates probed by fluorescence spectroscopy. Langmuir 18, 3829–3835.

Croy, S.R., Kwon, G.S., 2006. Polymeric micelles for drug delivery. Curr. Pharm. Des. 12, 4669–4684.

Daruwalla, J., Nikfarjam, M., Greish, K., Malcontenti-Wilson, C., Muralidharan, V., Christophi, C., Maeda, H., 2010. In vitro and in vivo evaluation of tumor targeting styrene–maleic acid copolymer-pirarubicin micelles: survival improvement and inhibition of liver metastases. Cancer Sci. 101, 1866–1874.

Fukuyo, Y., Hunt, C.R., Horikoshi, N., 2010. Geldanamycin and its anti-cancer activities. Cancer Lett. 290, 24–35.

Gaucher, G., Dufresne, M.H., Sant, V.P., Kang, N., Maysinger, D., Leroux, J.C., 2005. Block copolymer micelles: preparation, characterization and application in drug delivery. J. Control. Release 109, 169–188.

Ge, J., Normant, E., Porter, J.R., Ali, J.A., Dembski, M.S., Gao, Y., Georges, A.T., Grenier, L., Pak, R.H., Patterson, J., Sydor, J.R., Tibbitts, T.T., Tong, J.K., Adams, J., Palombella, V.J., 2006. Design, synthesis, and biological evaluation of hydroquinone derivatives of 17-amino-17-demethoxygeldanamycin as potent, water-soluble inhibitors of Hsp90. J. Med. Chem. 49, 4606–4615.

Gelderblom, H., Verweij, J., Nooter, K., Sparreboom, A., 2001. Cremophor® EL: the drawbacks and advantages of vehicle selection for drug formulation. Eur. J. Cancer 37, 1590–1598.

Greish, K., 2007. Enhanced permeability and retention of macromolecular drugs in solid tumors: a royal gate for targeted anticancer nanomedicines. J. Drug Target 15, 457–464.

Greish, K., Fang, J., Inutsuka, T., Nagamitsu, A., Maeda, H., 2003. Macromolecular therapeutics: advantages and prospects with special emphasis on solid tumour targeting. Clin. Pharmacokinet. 42, 1089–1105.

Greish, K., Sawa, T., Fang, J., Akaike, T., Maeda, H., 2004. SMA-doxorubicin, a new polymeric micellar drug for effective targeting to solid tumours. J. Control. Release 97, 219–230.

Gros, L., Ringsdorf, H., Schupp, H., 1981. Polymeric antitumor agents on a molecular and on a cellular level? Angew. Chem. Int. Ed. Engl. 20, 305–325.

Iyer, A.K., Greish, K., Fang, J., Murakami, R., Maeda, H., 2007. High-loading nanosized micelles of copoly(styrene-maleic acid)-zinc protoporphyrin for targeted delivery of a potent heme oxygenase inhibitor. Biomaterials 28, 1871–1881.

Kasuya, Y., Lu, Z.R., Kopeckova, P., Tabibi, S.E., Kopecek, J., 2002. Influence of the structure of drug moieties on the in vitro efficacy of HPMA copolymer-geldanamycin derivative conjugates. Pharm. Res. 19, 115–123.

Kelland, L.R., Sharp, S.Y., Rogers, P.M., Myers, T.G., Workman, P., 1999. DT-diaphorase expression and tumor cell sensitivity to 17-allylamino, 17-demethoxygeldanamycin, an inhibitor of heat shock protein 90. J. Natl. Cancer Inst. 91, 1940–1949.

Kobayashi, A., Oda, T., Maeda, H., 1988. Protein binding of macromolecular anticancer agent SMANCS: characterization of poly(styrene-co-maleic acid) derivatives as an albumin binding ligand. J. Bioact. Compat. Polym. 3, 319–333.

Larson, N., Ray, A., Malugin, A., Pike, D.B., Ghandehari, H., 2010. HPMA copolymer-aminohexylgeldanamycin conjugates targeting cell surface expressed GRP78 in prostate cancer. Pharm. Res. 27, 2683–2693.

Maeda, H., 2001. SMANCS and polymer-conjugated macromolecular drugs: advantages in cancer chemotherapy. Adv. Drug Deliv. Rev. 46, 169–185.

Matsumura, Y., Oda, T., Maeda, H., 1987. General mechanism of intratumor accumulation of macromolecules: advantage of macromolecular therapeutics. Gan To Kagaku Ryoho 14, 821–829.

Park, K., 2007. Nanotechnology: what it can do for drug delivery. J. Control. Release 120, 1–3.

Porter, J.R., Ge, J., Lee, J., Normant, E., West, K., 2009. Ansamycin inhibitors of Hsp90: nature's prototype for anti-chaperone therapy. Curr. Top. Med. Chem. 9, 1386–1418.

Rodriguez, V.B., Henry, S.M., Hoffman, A.S., Stayton, P.S., Li, X., Pun, S.H., 2008. Encapsulation and stabilization of indocyanine green within poly(styrene-alt-maleic anhydride) block-poly(styrene) micelles for near-infrared imaging. J. Biomed. Opt. 13, 014025.

Rowinsky, E.K., Donehower, R.C., 1995. Paclitaxel (taxol). N. Engl. J. Med. 332, 1004–1014.

Sausville, E.A., Tomaszewski, J.E., Ivy, P., 2003. Clinical development of 17-allylamino, 17-demethoxygeldanamycin. Curr. Cancer Drug Targets 3, 377–383.

Sharp, S., Workman, P., 2006. Inhibitors of the HSP90 molecular chaperone: current status. Adv. Cancer Res. 95, 323–348.

Shin, H.-C., Alani, A.W.G., Rao, D.A., Rockich, N.C., Kwon, G.S., 2009. Multi-drug loaded polymeric micelles for simultaneous delivery of poorly soluble anticancer drugs. J. Control. Release 140, 294–300.

Subr, V., Kopecek, J., Pohl, J., Baudys, M., Kostka, V., 1988. Cleavage of oligopeptide side-chains in N-(2-hydroxypropyl)methacrylamide copolymers by mixtures of lysosomal enzymes. J. Control. Release 8, 133–140.

Supko, J.G., Hickman, R.L., Grever, M.R., Malspeis, L., 1994. Preclinical pharmacologic evaulation of geldanamycin as an antitumor agent. Cancer Chemother. Pharmacol. 36, 305–315.

Suzuki, F., Munakata, T., Maeda, H., 1988. Interferon induction by SMANCS: a polymer-conjugated derivative of neocarzinostatin. Anticancer Res. 8, 97–103.

Suzuki, F., Pollard, R.B., Uchimura, S., Munakata, T., Maeda, H., 1990. Role of natural killer cells and macrophages in the nonspecific resistance to tumors in mice stimulated with SMANCS, a polymer-conjugated derivative of neocarzinostatin. Cancer Res. 50, 3897–3904.

Whitesell, L., Lindquist, S.L., 2005. HSP90 and the chaperoning of cancer. Nat. Rev. Cancer 5, 761–772.

Xiong, M.P., Yáñez, J.A., Kwon, G.S., Davies, N.M., Forrest, M.L., 2009. A cremophor-free formulation for tanespimycin (17-AAG) using PEO-*b*-PDLLA micelles: characterization and pharmacokinetics in rats. J. Pharm. Sci. 98, 1577–1586.

Zhong, Z., Licari, P.J., 2005. Pharmaceutical solution formulations containing 17-AAG. US Patent Application, 20,050,256,097.

0022-3565/11/3393-779–789$25.00
THE JOURNAL OF PHARMACOLOGY AND EXPERIMENTAL THERAPEUTICS

JPET 339:779–789, 2011

Vol. 339, No. 3
185348/3729805
Printed in U.S.A.

Therapeutic Potential of Pegylated Hemin for Reactive Oxygen Species-Related Diseases via Induction of Heme Oxygenase-1: Results from a Rat Hepatic Ischemia/Reperfusion Injury Model[S]

Jun Fang, Haibo Qin, Takahiro Seki,[1] Hideaki Nakamura, Kenji Tsukigawa, Takashi Shin, and Hiroshi Maeda

Laboratory of Microbiology and Oncology, Faculty of Pharmaceutical Sciences (J.F., H.Q., T.S., H.N., K.T.), Department of Applied Microbial Technology, Faculty of Biotechnology and Life Science (H.Q., T.S.), and DDS Research Institute (H.N., H.M.), Sojo University, Kumamoto, Japan

Received June 23, 2011; accepted September 2, 2011

ABSTRACT

Many diseases and pathological conditions, including ischemia/reperfusion (I/R) injury, are the consequence of the actions of reactive oxygen species (ROS). Controlling ROS generation or its level may thus hold promise as a standard therapeutic modality for ROS-related diseases. Here, we assessed heme oxygenase-1 (HO-1), which is a crucial antioxidative, antiapoptotic molecule against intracellular stresses, for its therapeutic potential via its inducer, hemin. To improve the solubility and in vivo pharmacokinetics of hemin for clinical applications, we developed a micellar hemin by conjugating it with poly(ethylene glycol) (PEG) (PEG-hemin). PEG-hemin showed higher solubility in water and significantly prolonged plasma half-life than free hemin, which resulted from its micellar nature with molecular mass of 126 kDa in aqueous media. In a rat I/R model, administration of PEG-hemin significantly elevated HO-1 expression and enzymatic activity. This induction of HO-1 led to significantly improved liver function, reduced apoptosis and thiobarbituric acid reactive substances of the liver, and decreased inflammatory cytokine production. PEG-hemin administration also markedly improved hepatic blood flow. These results suggest that PEG-hemin exerted a significant cytoprotective effect against I/R injury in rat liver by inducing HO-1 and thus seems to be a potential therapeutic for ROS-related diseases, including I/R injury.

Introduction

All aerobic organisms generate reactive oxygen species (ROS), which seem to be indispensable for signal transduction pathways that regulate cell growth and redox status (Davies, 1995). However, overproduction of these highly reactive metabolites can initiate lethal chain reactions and damage cell integrity and survival (Oda et al., 1989; Davies, 1995), which result in reversible and irreversible tissue injury. ROS are known to be involved in many diseases, for example, microbial infections, inflammation, ischemia/reperfusion (I/R) injury, neurological disorders, Parkinson's disease, hypertension, and cancer (Maeda and Akaike, 1991; McCord, 2000). Developing therapeutics for these ROS-related diseases by suppressing ROS generation or its levels in the body therefore seems to be a reasonable approach. Indeed, many research groups have used this rationale and

This work was supported in part by the Ministry of Education, Science, Culture, Sports, and Technology of Japan [Grants-in-Aid 17016076, 20015405]; and research funds from the Faculty of Pharmaceutical Sciences at Sojo University.

Part of this work was presented previously: Fang J, Qin H, Seki T, Nakamura H, Bharate GY, and Maeda H (2010) Pegylated hemin, a water-soluble micelle with therapeutic potential against ischemia-reperfusion injury via induction of heme oxygenase-1, at the *37th Annual Meeting and Exposition of the Controlled Release Society*; 2010 July 10–14; Portland, OR. Controlled Release Society, St. Paul, MN.

J.F. and H.Q. contributed equally to this work.

[1]Current affiliation: Laboratory of Angiogenesis Research, Department of Microbiology, Tumor and Cell Biology, Karolinska Institute, Stockholm, Sweden.

Article, publication date, and citation information can be found at http://jpet.aspetjournals.org.
doi:10.1124/jpet.111.185348.

[S] The online version of this article (available at http://jpet.aspetjournals.org) contains supplemental material.

ABBREVIATIONS: ROS, reactive oxygen species; HO, heme oxygenase; XO, xanthine oxidase; PEG, poly(ethylene glycol); EPR, enhanced permeability and retention; I/R, ischemia/reperfusion; TBARS, thiobarbituric acid reactive substance; PCR, polymerase chain reaction; ZnPP, zinc protoporphyrin; DLS, dynamic light scattering; AUC, area under the concentration versus time curve; Hc, hepatocytes; GAPDH, glyceraldehyde-3-phosphate dehydrogenase; SMA, styrene maleic acid; ALT, alanine aminotransferase; AST, aspartate aminotransferase; LDH, lactate dehydrogenase; TUNEL, terminal deoxynucleotidyl transferase dUTP nick-end labeling; 8-OHdG, 8-hydroxydeoxyguanosine; ELISA, enzyme-linked immunosorbent assay; MCP-1, monocyte chemotactic protein 1.

investigated various antioxidative agents and enzymes, such as superoxide dismutase and catalase (Oda et al., 1989; Muzykantov et al., 1996; Fang et al., 2009b). Inhibitors of the ROS-generating enzyme xanthine oxidase (XO) were also the targets along this line (Miyamoto et al., 1996; Fang et al., 2009a, 2010).

In addition to these enzymes, heme oxygenase-1 (HO-1), the antioxidative, antiapoptotic molecule, has attracted great attention. HO is the key enzyme in heme degradation, which generates biliverdin, carbon monoxide (CO), and free iron (Fe^{2+}) (Maines, 1988; Fang et al., 2004). Biliverdin is subsequently reduced by cytosolic biliverdin reductase to form bilirubin, a potent antioxidant (Baranano et al., 2002). In addition, reports have shown that CO contributes in regulating vascular tone and exhibits antioxidative, anti-inflammatory, and antiapoptotic properties (Abraham and Kappas, 2008). HO-1 is the inducible form of HO, which is a member of the heat shock protein family (Hsp32), and its expression is believed to be associated with fundamental adaptive and defensive responses to oxidative stress and cell stress (Doi et al., 1999; Fang et al., 2004; Abraham and Kappas, 2008). Therefore, induction of HO-1 may become an effective therapeutic strategy for ROS-related diseases. Among HO-1 inducers, hemin is one of the most potent and has few adverse effects to the host. In fact, hemin is used to treat acute hepatic porphyria in Europe and the United States.

However, the very poor water solubility of hemin makes it difficult to achieve a clinically effective dose and develop an optimal therapeutic protocol. To overcome this drawback, we prepared a water-soluble micellar form of hemin by using the biocompatible polymer poly(ethylene glycol) (PEG) (PEG-hemin). This polymer conjugation resulted in an increased in vivo half-life ($t_{1/2}$) and reduced antigenicity, as reported previously (Sawa et al., 2000; Fang et al., 2003), and improves pharmacological efficacy significantly.

I/R injury, a typical ROS-related pathological process, is a major cause of organ damage in many fatal diseases such as cardiac infarction, cerebral ischemia, and thrombosis, as well as in surgical procedures. Many studies reported that ROS, especially superoxide anion radical (O_2^-), is produced excessively in many tissues, mostly by XO, during I/R injury (McCord, 1985). Under normal conditions most XO is present as xanthine dehydrogenase type D, which has very low O_2^--generating activity; however, during ischemia, XO activity rapidly increases by conversion from XO type D to type O, which leads to rapid production of O_2^- (Roy and McCord, 1983). O_2^-, with highly cytotoxic activity, is converted to H_2O_2 by superoxide dismutase, and then to hydroxyl radicals in the presence of transition metals (e.g., Fe^{2+}), if no catalase is available. All of these ROS can readily cross cell membranes and cause oxidative damage to DNA, proteins, and lipids (Halliwell and Gutteridge, 1984; Beckman and Ames, 1997; Berlett and Stadtman, 1997). In addition, O_2^- can react rapidly with NO and form the more toxic species peroxynitrite ($ONOO^-$), which further exacerbates tissue injury or leads to complications. Furthermore, removal of NO by reactions with O_2^- on the vascular endothelial surface results in vasoconstriction (hypertension) and triggers neutrophil adherence and accumulation, which will exacerbate reperfusion injury (Beckman and Koppenol, 1996; Akaike and Maeda, 2000). All of these data together indicate that ROS are the major cause of I/R-induced tissue injury and subsequent pathological manifestations.

The present study describes the synthesis of PEG-hemin and the physicochemical and biological characterization of the conjugate. In view of the therapeutic potential of this agent for ROS-related diseases, this study also evaluated the cytoprotective effect of PEG-hemin in vivo in a rat liver I/R model.

Materials and Methods

Materials. Hemin was purchased from Sigma-Aldrich (St. Louis, MO). The succinimidyl glutarate derivative of PEG (MEGC-50HS), with a mean molecular weight of 5250, was from NOF Co. (Tokyo, Japan). PEG used in this experiment had a molecular weight dispersity index of 1.025. Other chemicals of reagent grade were from Wako Pure Chemicals (Osaka, Japan) and used without additional purification.

Cell Culture. Human hepatocyte Hc cells (DS Pharma Biomedical Co. Ltd, Osaka, Japan) were cultured in CSC Serum-Free Medium (DS Pharma Biomedical Co. Ltd) at 37°C in a 5% CO_2/95% air atmosphere.

Animals. Male Wistar rats, 6 to 7 weeks old and weighing between 200 and 230 g, and 6-week-old male *ddY* mice, weighing between 20 and 25 g, were obtained from Kyudo Inc. (Kumamoto, Japan). All animals were maintained under standard conditions and fed water and murine chow ad libitum. All experiments were carried out according to the guidelines of the Laboratory Protocol of Animal Handling, Faculty of Pharmaceutical Sciences, Sojo University.

Synthesis of PEG-Hemin. PEG-hemin was synthesized according to the protocol for PEG-zinc protoporphyrin (PEG-ZnPP) synthesis described in our previous work (Sahoo et al., 2002), with some modifications. In brief, an aminated derivative of hemin was synthesized by using ethylenediamine, and then succinimidyl PEG was cross-linked to hemin via the amide bond (Scheme 1). The resultant PEG-hemin was characterized by means of a UV spectrophotometer (model UV/Vis-550; Jasco, Tokyo, Japan) and infrared spectrometer (FT/IR-4200; Jasco), as well as dynamic light scattering (DLS) and Sephadex column chromatography, as described below.

Quantification of the Free Amino Group. To determine whether PEG reacted with the amino group introduced into hemin, loss of the primary amino group after the reaction was quantified by the use of fluorescamine, an amino group-reactive fluorescent agent (Stocks et al., 1986). In brief, 2 μM PEG-hemin (hemin equivalent) and diethylaminohemin (aminated derivative of hemin) were dissolved in deionized water and then reacted with fluorescamine. Fluorescence was detected at 475 nm with excitation at 390 nm. The concentration of free amino groups in PEG-hemin was estimated by using glycine as the standard.

Size Exclusion Chromatography. Size exclusion chromatography was performed with a Sephadex G-100 column, 40 cm (length) × 1.3 cm (diameter) (GE Healthcare, Chalfont St. Giles, Buckinghamshire, UK), to determine the apparent molecular mass of PEG-hemin. Various globular proteins of known molecular mass were used as reference standards. The mobile phase was 0.25 M $NaHCO_3$, pH 8.2, and 2.5-ml fractions were collected per tube.

DLS Measurement of PEG-Hemin Particle Size. DLS measurement was performed with the Photal DLS-7000 HLs laser spectrophotometer (Otsuka Electronics, Osaka, Japan), equipped with a 10-mW He/Ne laser, at a wavelength of 632.8 nm. The scattering angle was fixed at 90°, and the temperature was at 25°C ± 0.05°C. Particle size was determined with 0.1 mg/ml samples prepared in deionized water (filtered through a 0.45-μm filter).

In Vivo Pharmacokinetics of PEG-Hemin. *ddY* mice were used in the determination of PEG-hemin plasma $t_{1/2}$, area under the concentration versus time curve (AUC), and total body clearance. PEG-hemin (dissolved in physiological saline) or free hemin (dissolved in 0.01 M NaOH with 10% dimethyl sulfoxide) was injected intravenously at 10 mg/kg (hemin equivalent). After scheduled in-

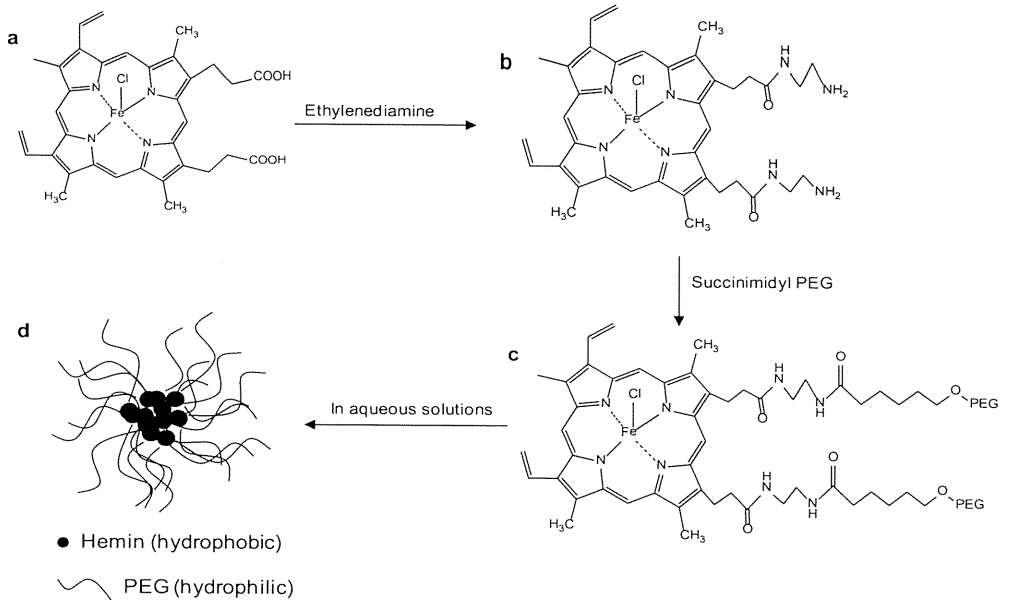

Scheme 1. Synthesis and chemical structure of PEG-hemin. a and b, an amino group was introduced into hemin (a; $C_{34}H_{32}ClFeN_4O_4$) by using ethylenediamine, which resulted in bis(ethylenediamino) hemin (b; $C_{38}H_{46}ClFeN_8O_2$), which was pegylated via succinimidyl PEG. c and d, the resultant PEG-hemin [c; $CH_3O(CH_2CH_2O)_n$-CO-$CH_2CH_2CH_2$-CO- $C_{38}H_{45}ClFeN_8O_2$] formed micelles (d) in aqueous solutions.

tervals, mice were killed and blood was collected in the presence of heparin, so that plasma could be obtained after centrifugation at 5000*g* for 20 min at 4°C. Then, 1.8 ml of ethanol with 0.25 M HCl was added to 0.2 ml of plasma to extract PEG-hemin or hemin. After vigorous vortexing and centrifugation at 20,000*g* for 20 min, supernatant UV spectra between 300 and 600 nm were measured, and peak absorbance at 385 nm was used to calculate the concentration of hemin according to the standard curve of hemin.

In Vitro Cytotoxicity Assay of PEG-Hemin. Human hepatocytes (Hc) were plated at 3000 cells/well in a 96-well plate (NUNC A/S, Roskilde, Denmark). After overnight preincubation, different concentrations of PEG-hemin were added to the cells. After an additional 48-h incubation, cell viability was determined by using the 3-(4,5-dimethylthiazol-2-yl)-2,5-diphenyltetrazolium bromide assay (Dojindo Laboratories, Kumamoto, Japan).

Induction of HO-1 Expression in Human Hepatocytes by PEG-Hemin. To investigate the HO-1-inducing activity of PEG-hemin, HO-1 expression in human Hc was determined with or without PEG-hemin treatment. Hc cells were plated in six-well culture plates (50,000 cells/well), incubated overnight at 37°C, and treated with the indicated concentrations of PEG-hemin for 24 h. Cells were then collected, and total RNA and protein were extracted by using TRIzol reagent (Invitrogen, Carlsbad, CA) and CelLytic MT (Sigma-Aldrich) reagent, according to the manufacturers' instructions. Reverse transcription-PCR was performed for quantification of HO-1 copies in Hc cells. Primers used for PCR were as follows: HO-1 antisense 21-mer, 5′-GATGTTGAGCAGGAACGCGAT-3′, and HO-1 sense 21-mer, 5′-CAGGCAGAGAATGCTGAGTTC-3′, to obtain a 555-bp HO-1 cDNA (nucleotides 79–633); and GAPDH antisense 24-mer, 5′-CATGTGGGCCATGAGGTCCACCAC-3′, and sense 26-mer, 5′-TGAAGGTCGGAGTCAACGGATTTGGT-3′, to obtain a 983-bp GAPDH cDNA fragment. After an initial denaturing step at 94°C, 25 PCR cycles (30 cycles for GAPDH) were performed as follows: denaturing for 1 min at 94°C, primer annealing for 1 min at 56°C, and DNA synthesis for 1 min at 72°C. PCR products then underwent electrophoresis on ethidium bromide-stained 1% agarose gels.

Experimental Protocol for Hepatic I/R Injury. Rats were fasted overnight before the experiment but were allowed free access to water. Animals were anesthetized with isoflurane during the operation by using an anesthesia system (SF-B01; DS Pharma Biomedical Co. Ltd). After the abdomen was shaved and disinfected with 70% ethanol, a complete midline incision was performed. The portal vein and hepatic artery were exposed and cross-clamped for 30 min with a noncrushing microvascular clip. Subsequently, reperfusion was initiated by removing the clips, and the abdomen was closed in two layers with 2-0 silk. Rats were kept warmed until they awoke and became active. Two hours before surgery for I/R, saline or PEG-hemin at different doses (2 or 10 mg/kg) was injected into each rat via the tail vein. In some experiments, a polymeric micellar HO-1 inhibitor, ZnPP, encapsulated with styrene maleic acid (SMA) copolymer, namely SMA-ZnPP (Iyer et al., 2007), was administered intravenously (5 mg/kg) just before I/R.

Measurement of Liver Enzyme Activity in Serum. Three hours after reperfusion resumed, rats were killed under anesthesia, and whole blood was withdrawn from the inferior vena cava. Activities of alanine aminotransferase (ALT), aspartate aminotransferase (AST), and lactate dehydrogenase (LDH) in serum were determined by means of the AutoAnalyzer system (Hitachi Ltd., Tokyo, Japan). Activities were expressed as IU/l.

Measurement of HO-1 Expression and Activity in Rat Liver after I/R. Liver tissues collected from rats receiving the above-described treatment with PEG-hemin or no treatment were homogenized with a Polytron homogenizer (Kinematica, Littau-Lucerne, Switzerland) in ice-cold homogenizing buffer (20 mM potassium phosphate buffer, pH 7.4, plus 250 mM sucrose, 2 mM EDTA, 2 mM phenylmethylsulfonyl fluoride, and 10 μg/ml leupeptin). Homogenates were centrifuged at 10,000*g* for 30 min at 4°C, and the resultant supernatant was ultracentrifuged at 105,000*g* for 1 h at 4°C. The microsomal fraction in the precipitates was suspended in 0.1 M potassium phosphate buffer, pH 7.4, followed by sonication for 2 s at 4°C.

Supernatant of the 10,000*g* fraction, with 50 μg of protein in each sample, was used for analysis of HO-1 expression by Western blot. In brief, total protein was separated by electrophoresis with 12% SDS-polyacrylamide gels and transferred to Immobilon polyvinylidene difluoride membranes (Millipore Corporation, Billerica, MA). This process was followed by reaction with a monoclonal antibody for HO-1 (GTS-1; Takara Bio Inc., Otsu, Shiga, Japan). The protein band that reacted immunologically with the antibodies was visualized by using the enhanced chemiluminescence system (GE Healthcare).

The microsomal fraction was used for measurement of HO-1 activity. The HO reaction mixture consisted of the microsomal fraction (1 mg of protein), cytosolic fraction (supernatant after ultracentrifugation described above) of rat liver (1 mg of protein) as a source of biliverdin reductase, 33 μM hemin, and 333 μM NADPH in 1 ml of 0.1 M potassium phosphate buffer, pH 7.4. The mixture was incubated for 15 min at 37°C, after which the reaction was terminated by addition of 33 μl of 0.01 M HCl. Bilirubin formed in the reaction was extracted with 1.0 ml of chloroform, and bilirubin concentration was

determined spectroscopically by measuring the difference in absorbance between 465 nm (absorbance of bilirubin) and 530 nm (background), with a molar extinction coefficient of 40 $mM^{-1} \cdot cm^{-1}$ at 465 nm.

Moreover, HO-2 expression in this experimental protocol was measured by reverse transcription-PCR. In brief, total RNA of each liver tissue was extracted by using TRIzol reagent (Invitrogen) according to the manufacturers' instructions. Primers used for PCR were as follows: antisense, 5′-AGTAAAGTGCAGTGGTGGCC3-′, and sense, 5′-CAGCAACAATGTCTTCAGAGG-3′ to obtain a 230-bp HO-2 cDNA. After an initial denaturing step at 94°C, 35 PCR cycles were performed as follows: denaturing for 2 min at 92°C, primer annealing for 1 min at 54°C, and DNA synthesis for 1 min at 72°C. PCR products then underwent electrophoresis on ethidium bromide-stained 1% agarose gels.

Quantification of CO in Blood. After the I/R procedure just described, rats were killed and blood was collected. Each 0.35-ml sample of blood was diluted with 3.65 ml of phosphate-buffered saline and placed in a 10-ml glass test tube on ice. The test tubes were then sealed, and the air in the tubes was replaced by purging nitrogen gas into the tubes, after which the NO donor 3-(2-hydroxy-1-methyl-2-nitrosohydrazino)-*N*-methyl-1-propanamine was added, to a final concentration of 1 mM. Because NO has a much higher affinity than CO for hemoglobin, CO bound to hemoglobin would be liberated. After 2 h of incubation at room temperature, 1 ml of the gas in the test tubes was collected and processed in a gas chromatography CO analyzer (TRIlyzer mBA-3000; TAIYO Instruments, Inc., Osaka, Japan) equipped with a semiconductor gas sensor.

Preparation of Liver Tissue Sections for Histological Examination and Detection of Apoptosis. Rat livers were collected 3 h after I/R and cut into small tissue blocks (approximately 3–5 mm in length, width, and height). After the blocks were fixed with 6% buffered neutral formalin solution, they were embedded in paraffin. Paraffin-embedded sections (6 μm thick) were prepared as usual for histological examination after hematoxylin and eosin staining and for apoptosis staining (TUNEL) as described below.

In Situ Detection of Apoptosis in the Liver. TUNEL staining was used to investigate apoptosis in the paraffin-embedded sections described above, after I/R with or without PEG-hemin treatment, with an in situ apoptosis detection kit (TACS; Trevigen, Gaithersburg, MD), according to the manufacturer's instructions. TUNEL-positive cells in four different fields per sample were counted, and results were expressed per mm^2 of tissue section.

Detection of Caspase 3/7 Activities in the Liver. Apoptosis in the livers of different treatment groups were further examined in their caspase 3/7 activities, with a caspase assay kit that contains the substrate peptide DEVD (Caspase-Glo 3/7 Assay; Promega, Madison, WI). In brief, the liver tissue homogenates were prepared by using 1 g of wet tissue added with 4 ml of hypotonic extraction buffer (25 mM HEPES buffer, pH 7.5, 5 mM $MgCl_2$, 1 mM EGTA, 2 mM phenylmethylsulfonyl fluoride, and 10 μg/ml leupeptin) with the Polytron homogenizer (Kinematica). Homogenates were centrifuged at 10,000*g* for 30 min at 4°C, and the supernatant was used for caspase activity assay according to the manufacturer's instructions.

Measurement of Liver Tissue Blood Flow. A laser Doppler flowmeter (ALF21; Advance Co. Ltd., Tokyo, Japan) was used to measure liver tissue blood flow in anesthetized animals during I/R (until 1 h after initiating reperfusion) with or without PEG-hemin treatment (10 mg/kg i.v.). The flowmeter probe was inserted at the same site in the median lobe of the liver in each animal. The real-time change in blood flow was monitored, and the mean blood flow at specific time points was calculated and expressed as a percentage of the preischemic initial blood flow value as the control.

Thiobarbituric Acid-Reactive Substance Assay. Oxidative cell damage in the liver after I/R with or without PEG-hemin treatment was quantified by assay of lipid peroxide formation via the thiobarbituric acid reaction (Ohkawa et al., 1979). In brief, liver tissue homogenates were prepared at a ratio of 1 g of wet tissue to 9 ml of 1.15% KCl in a Polytron homogenizer. Then, 0.1 ml of homogenate was mixed with 0.2 ml of 8.1% SDS, 1.5 ml of 20% acetic acid (pH 3.5 adjusted with NaOH), and 1.5 ml of a 0.8% aqueous solution of thiobarbituric acid. The final sample was made up to 4 ml with distilled water and incubated at 95°C for 60 min. After cooling with tap water, 1.0 ml of distilled water and 5.0 ml of a mixture of *n*-butanol and pyridine (15:1, v/v) were added, and each reaction mixture was shaken vigorously. After centrifugation at 5000*g* for 10 min, absorbance of the organic upper layer was measured at 532 nm.

ELISA for 8-Hydroxydeoxyguanosine in the Liver. Oxidative injury of the liver after I/R with or without PEG-hemin treatment was further examined by detecting 8-hydroxydeoxyguanosine (8-OHdG) in liver tissues, by use of an ELISA kit (8-OHdG Check; JalCA, Fukuroi, Shizuoka, Japan). In brief, DNA in each sample was extracted by using a QuickGene DNA tissue kit (DT-S; Wako Pure Chemicals), followed by hydrolysis using an 8-OHdG Assay Preparation Reagent Set (Wako Pure Chemicals). The ELISA was then performed to detect 8-OHdG according to the manufacturer's instructions.

ELISA for Monocyte Chemotactic Protein 1 in Serum. Serum samples from I/R-treated rats were obtained as described above, and the monocyte chemotactic protein 1 (MCP-1) levels were quantified by using an ELISA kit (Immuno-Biological Laboratories Co., Ltd., Takasaki-Shi, Gunma, Japan) according to the manufacturer's instructions.

Statistical Analysis. All data are expressed as means ± S.E. Student's *t* test was used to determine the significance between each experimental group. A difference was considered statistically significant when $P < 0.05$.

Results

Synthesis of PEG-Hemin. As we reported previously, to facilitate conjugation of hemin with PEG we first conjugated with ethytlenediamine to generate amino groups onto two carboxyl groups in the porphyrin ring of hemin, to produce more reactive nucleophiles than the original carboxyl group (Sahoo et al., 2002). Then, pegylation targeted to the amino groups was successfully achieved by using succinimidyl-activated PEG, with two PEG chains conjugated to the porphyrin structure of hemin (Scheme 1). The resulting PEG-hemin exhibited a high water solubility, more than 15 mM, whereas native hemin is almost insoluble in water or physiological solutions. Physiochemical analysis showed that PEG-hemin had a UV spectrum that was similar to that of free hemin (data not shown). IR spectra of PEG-hemin exhibited a characteristic absorption of amide bonds at 1654 cm^{-1} (amide I) and 1542 cm^{-1} (amide II) (Fig. 1), which demonstrated conjugation between PEG and hemin via amide bonds. Cross-link of PEG was further supported by the fact that PEG-hemin had no free amino groups after pegylation (Scheme 1), as determined by fluorescamine (data not shown).

The molecular mass of PEG-hemin, as calculated from the chemical structure of PEG-hemin shown in Scheme 1, was 10 to 12 kDa with two PEG molecules (approximately 5000 Da each) conjugated per mole of hemin. However, in aqueous solutions, PEG-hemin had a large molecular mass, approximately 126 kDa as analyzed by Sephadex G-100 column chromatography (Fig. 2A). This result was confirmed by DLS, which showed a mean particle size of 121.5 nm in deionized water (Fig. 2B). The particle size of PEG-hemin in water remained unchanged at 4°C for more than 1 month. These data clearly indicated the formation of stable micelles of PEG-hemin in aqueous solution, with the hydrophobic core assembly of hemin inside and the hydrophilic PEG outside (Scheme 1).

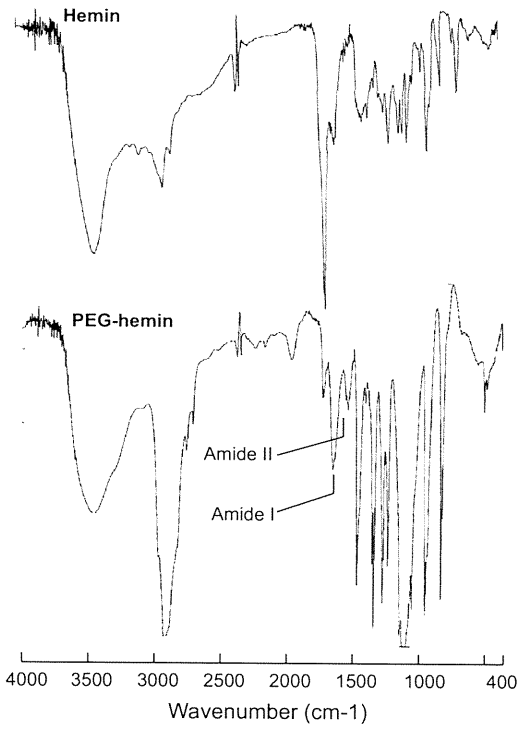

Fig. 1. IR spectra of hemin and PEG-hemin. Amide I (1654 cm^{-1}) and amide II (1542 cm^{-1}) were clearly observed in PEG-hemin, which suggested an amide bond formation between hemin and PEG through bis-(ethylenediamino) hemin.

Plasma $t_{1/2}$ of PEG-Hemin. We expected the macromolecular micellar formulation of PEG-hemin to have superior in vivo pharmacokinetics (e.g., prolonged $t_{1/2}$), and we investigated this possibility by using *ddY* mice. Compared with free hemin, PEG-hemin had a relatively long circulation time: even 20 h after intravenous injection, approximately 30% remained in circulation; almost no hemin was detected 2 h after administration (Fig. 3). The $t_{1/2}$ of PEG-hemin was calculated to be 18.2 h, which is approximately 20 times longer than that of hemin (0.96 h); in parallel, the AUC of PEG-hemin increased to 16 times of that of free hemin, and the total body clearance of PEG-hemin was approximately 16 times slower than that of free hemin (Table 1).

In Vitro Cytotoxicity and HO-1 Induction Activity of PEG-Hemin. Figure 4A shows no apparent cytotoxicity for PEG-hemin up to 250 μM (hemin equivalent). More important, PEG-hemin treatment significantly induced expression of HO-1 mRNA in cultured human hepatocytes (Fig. 4B).

In Vivo HO-1 Induction by PEG-Hemin in a Rat Liver I/R Model. The I/R procedure alone increased HO-1 protein expression in the liver tissue, but more important, this HO-1 expression was dramatically up-regulated by PEG-hemin treatment (Fig. 5A). Likewise, HO-1 activity in liver tissue, as assessed by the production of bilirubin, increased after I/R but more significantly increased after I/R plus PEG-hemin treatment (Fig. 5B). These findings were supported by the PEG-hemin-induced significant increase in the blood concentration of CO, which is another major product of HO-1-catalyzed heme degradation (Fig. 5C).

In addition, I/R procedure induced a slight increase of HO-2 expression; however, PEG-hemin treatment did not affect HO-2 expression (Supplemental Fig. 1).

Amelioration of Liver I/R Injury by PEG-Hemin. The potential therapeutic or tissue protective effect of PEG-hemin against I/R injury of the liver was evaluated by measuring plasma concentrations of the liver enzymes AST, ALT, and LDH. In our previous study, we reported that these enzymes increased to a maximum level at 3 h after reperfusion (Ikebe et al., 2000); thus, in this study all experiments were performed at 3 h after reperfusion. As anticipated, I/R caused a large increase in the levels of all three liver enzymes, to more than 20 times of normal levels. AST, ALT, and LDH values for I/R versus those for normal rat were as follows: 2647.4 ± 460.4 IU/l versus 65.3 ± 0.7 IU/l, 1356.4 ± 182.1 IU/l versus 54.3 ± 1.2 IU/l, and 6932.6 ± 1131.0 IU/l versus 62.3 ± 3.4 IU/l, respectively) (Fig. 6A).

More important, PEG-hemin treatment, at 10 mg/kg (hemin equivalent), significantly lowered the elevated levels of AST, ALT, and LDH, with liver enzyme levels almost recovering to normal (Fig. 6A). Furthermore, this cytoprotective effect of PEG-hemin was almost nullified by administration of SMA-ZnPP, which is a macromolecular water-soluble HO inhibitor that we had prepared previously (Iyer et al., 2007) (Fig. 6A). These results suggest that the cytoprotective effect of PEG-hemin was through an HO-1-mediated pathway, as

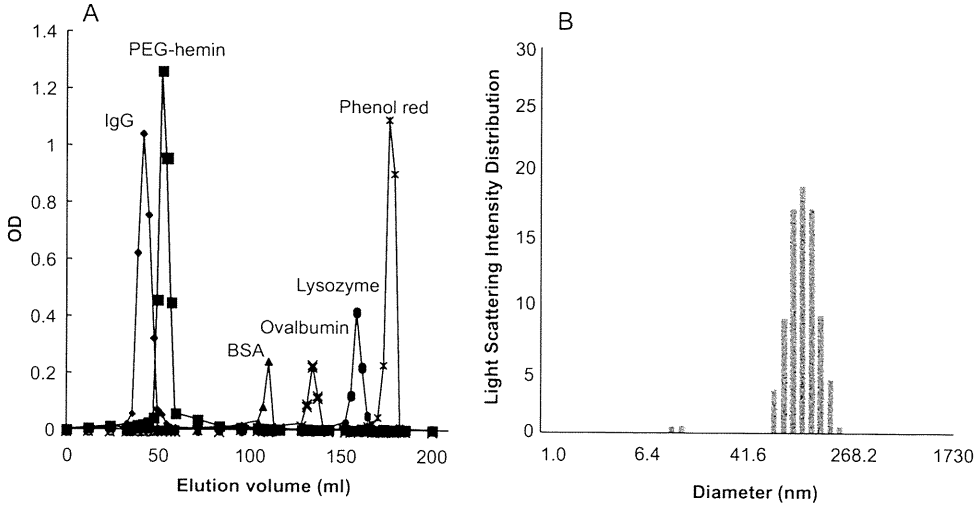

Fig. 2. Apparent molecular mass of PEG-hemin in aqueous solutions as analyzed by Sephadex G-100 gel chromatography (A) and DLS (B). Gel chromatography was performed with the mobile phase of 0.25 M $NaHCO_3$, pH 8.2, and the molecular mass of PEG-hemin in aqueous solutions was calculated by reference to known molecular mass protein markers. See *Synthesis of PEG-Hemin* under *Results* for details. BSA, bovine serum albumin.

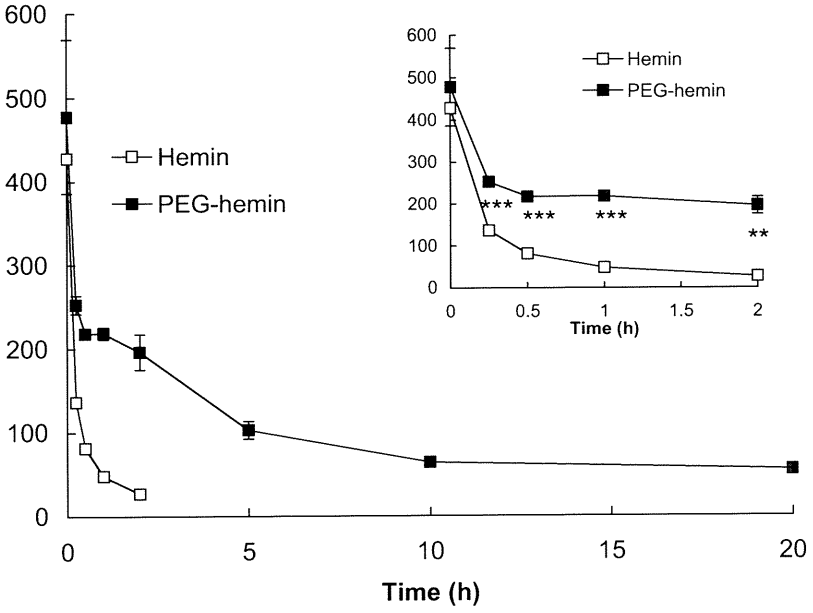

Fig. 3. Pharmacokinetics of PEG-hemin and native hemin in the blood of *ddY* mice. Native hemin or PEG-hemin was injected intravenously into *ddY* mice via the tail vein. After scheduled intervals, mice were killed, blood was collected, and blood concentrations of hemin and PEG-hemin were measured as described under *Materials and Methods*. Values are means ± S.E. ($n = 4$). **, $P < 0.01$; ***, $P < 0.001$, PEG-hemin versus native hemin.

TABLE 1
Pharmacokinetic parameters of free hemin and PEG-hemin
Plasma $t_{1/2}$ indicates time required to reach to half-concentration at time zero by interpolation.

Agent	$t_{1/2}$	AUC	Total Body Clearance
	h	*μg/ml/h*	*l/h/kg*
Hemin	0.96	203.3	49.2
PEG-hemin	18.25	3289.3	3.0

discussed in the *Introduction*. Consistent with these findings, hematoxylin and eosin staining of liver tissues after I/R revealed apparent necrotic areas, but necrosis was significantly inhibited by PEG-hemin treatment (Fig. 6B). In addition, rats not undergoing I/R showed no apparent changes in serum AST, ALT, and LDH values after injection of PEG-hemin (data not shown), which suggests that PEG-hemin seemed to be nontoxic to the liver.

Changes in Hepatic Blood Flow. One major reason for liver tissue injury by I/R is reduced blood flow, as clearly seen in Fig. 7, which shows that hepatic blood flow decreased to 20% of normal at 20 min after ischemia and recovered to only 30% of normal at 1 h after reperfusion was initiated. The tissue-protective effect of PEG-hemin was believed to result, at least in part, from improved hepatic blood flow. PEG-hemin treatment largely increased hepatic blood flow, which reached 80% of normal at 1 h after the start of reperfusion (Fig. 7).

Apoptosis in the Liver after I/R. The TUNEL assay for apoptosis allowed further elucidation of the pathological events caused by I/R with or without PEG-hemin treatment. I/R clearly induced apoptosis at 3 h after reperfusion, whereas PEG-hemin significantly lowered the number of apoptotic cells in the liver after I/R (Fig. 8A), findings that correlated well with the liver enzyme profiles. This was further supported by caspase 3/7 activity assay, by which the caspase 3/7 activities were found to be remarkably increased in the livers of I/R, whereas it was significantly inhibited by PEG-hemin (Fig. 8B).

Oxidative Injury Induced by I/R in the Liver. To investigate the role of ROS in liver I/R injury, the TBARS assay, which is a standard method of detecting oxidative injury of tissue involving lipid peroxidation, was performed. As Fig. 9 shows, I/R greatly increased the TBARS level in the rat liver. This increase was markedly inhibited by PEG-hemin treatment in a dose-dependent manner (Fig. 9): at 10 mg/kg PEG-hemin, the TBARS value was almost normal, which suggests that liver injury caused by I/R involved the increased generation of ROS. Similar results were obtained when 8-OHdG, which is a common index for oxidative injury of DNA, was detected in the liver of rat after I/R procedure with or without PEG-hemin treatment. These findings indicate the involvement of ROS in I/R injury and the protective effect of PEG-hemin in this process.

Change in Serum Inflammatory Cytokine MCP-1 Level after I/R With or Without PEG-Hemin. Inflammation is a major consequence of ROS-related diseases and thus plays a crucial role in the pathological process of I/R. Among the many inflammatory cytokines known to be involved in I/R injury, MCP-1, a proinflammatory chemokine and key mediator in the inflammatory process, is strongly associated with ROS-induced pathological conditions including I/R injury (Melgarejo et al., 2009). We thus measured the levels of MCP-1 in rat serum after I/R with or without PEG-hemin administration. Figure 10 shows a significantly increased serum MCP-1 level at 3 h after I/R. However, PEG-hemin treatment before I/R markedly inhibited this increase, which was consistent with the liver function results, as well as necrosis and apoptosis in liver tissue.

Discussion

During the past few decades, the clinical importance of ROS has been discussed extensively, and development of drugs to control the generation of ROS or scavenge ROS has become a focus of great interest (Maeda and Akaike, 1991; McCord, 2000). One approach is to block ROS generation. We in fact developed an XO inhibitor, 4-amino-6-hydroxypyrazolo[3,4-*d*]pyrimidine, and its polymer conjugate to inhibit O_2^- production by XO (Miyamoto et al., 1996; Fang et al., 2009a, 2010). An alternative approach that has attracted our

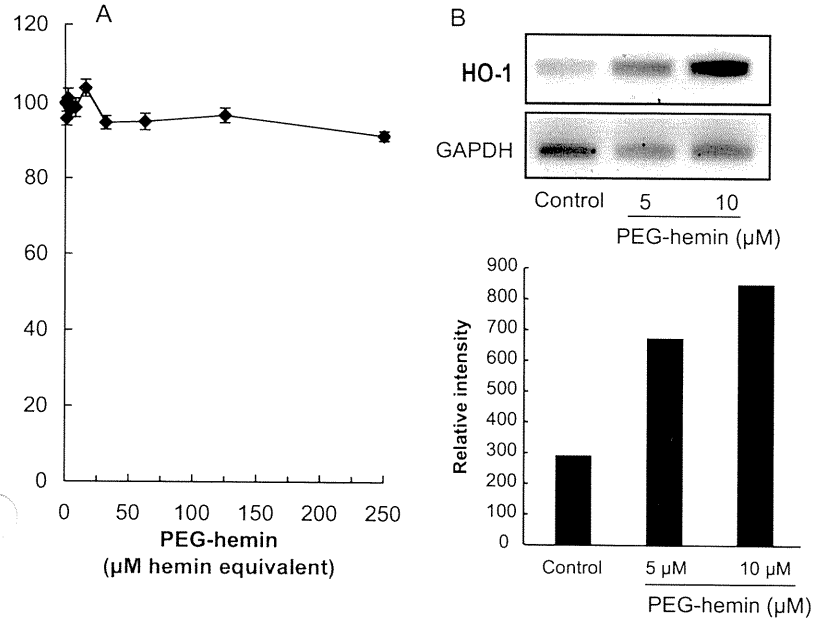

Fig. 4. In vitro cytotoxicity (A) and HO-1 induction activity (B) of PEG-hemin. The viability of human Hc was determined by using the 3-(4,5-dimethylthiazol-2-yl)-2,5-diphenyltetrazolium bromide assay. Values are means ± S.E. (n = 8 wells). See *In Vitro Cytotoxicity and HO-1 Induction Activity of PEG-Hemin* under *Results* for details.

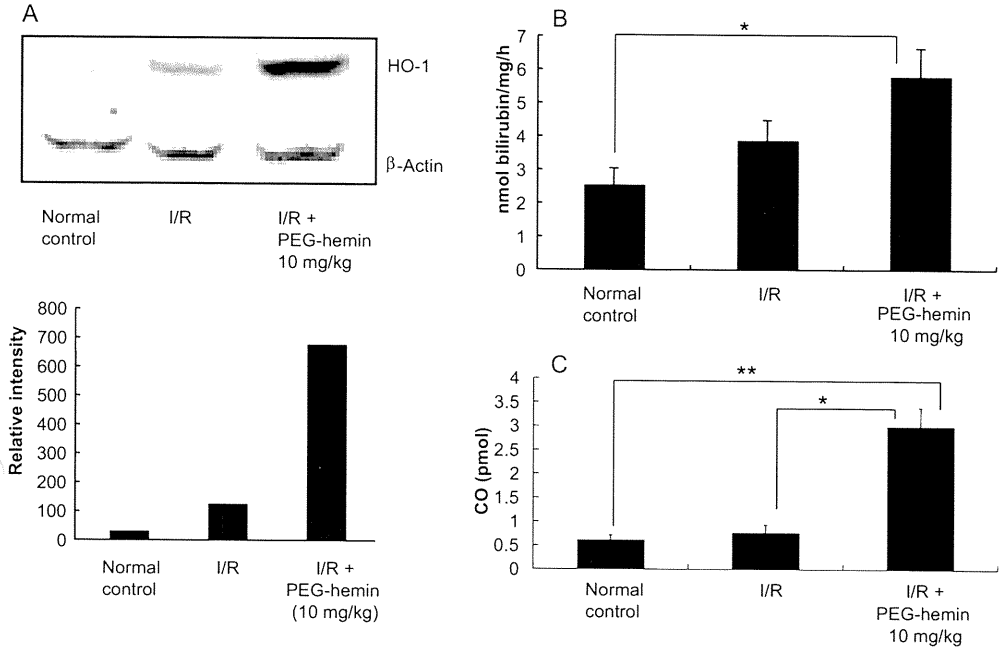

Fig. 5. In vivo induction of HO-1 by PEG-hemin in a rat I/R model. A and B, Western blot analysis for HO-1 protein in liver tissue (A) and HO-1 activity, as evidenced by bilirubin formation, in liver tissue after I/R with or without PEG-hemin treatment (B). C, HO-1 induction was further verified by measuring the CO concentration in blood. See *In Vivo HO-1 Induction by PEG-Hemin in a Rat Liver I/R Model* under *Results* for details. All data are presented as means ± S.E. (n = 4). *, $P < 0.05$; **, $P < 0.01$.

attention is to take advantage of the products of HO-1, which is a major antiapoptotic antioxidative molecule (Maines, 1988; Fang et al., 2004; Abraham and Kappas, 2008). Induction of HO-1 either by its inducers such as cobalt protoporphyrin and hemin or by HO-1 gene transfer showed beneficial effects in many ROS-related diseases (Fang et al., 2004; Abraham and Kappas, 2008). We followed this approach by using a modified hemin and developed a macromolecular micellar hemin formulation to improve its water solubility and in vivo pharmacokinetics.

We used PEG, which is a widely used biocompatible polymer, to prepare hemin micelles. Consistent with our previous reports of PEG-ZnPP (Sahoo et al., 2002; Fang et al., 2003), which is chemically similar to PEG-hemin, PEG modification of hemin led to markedly increased solubility (more than 15 mM; hemin equivalent) in physiological solutions, in which free hemin can be hardly solubilized. More important, PEG-hemin exhibited a very long circulation time: its $t_{1/2}$ in *ddY* mice was approximately 18 h, which was approximately 20 times longer than that of free hemin (Fig. 3; Table 1). Furthermore, PEG-hemin had no or very little toxicity; PEG-hemin treatment, up to 250 μM, produced no cell death (Fig. 4A). Its safety was also verified in vivo: injection of 100 mg/kg i.v. PEG-hemin into *ddY* mice did not cause the death of the mice or any apparent side effects such as loss of body weight and change in blood biochemistry (data not shown). These findings warrant further clinical applications of PEG-hemin.

The improved water solubility and plasma $t_{1/2}$ are caused by the micellar formulation of PEG-hemin, which had an apparent molecular mass of 126 kDa in aqueous solution as judged by Sephadex G-100 column chromatography (Fig. 2A). This PEG-hemin presents as an aggregated micellar form, as observed by DLS, which showed a mean particle size of 121.5 nm in physiological solution (Fig. 2B). Macromolecular drugs

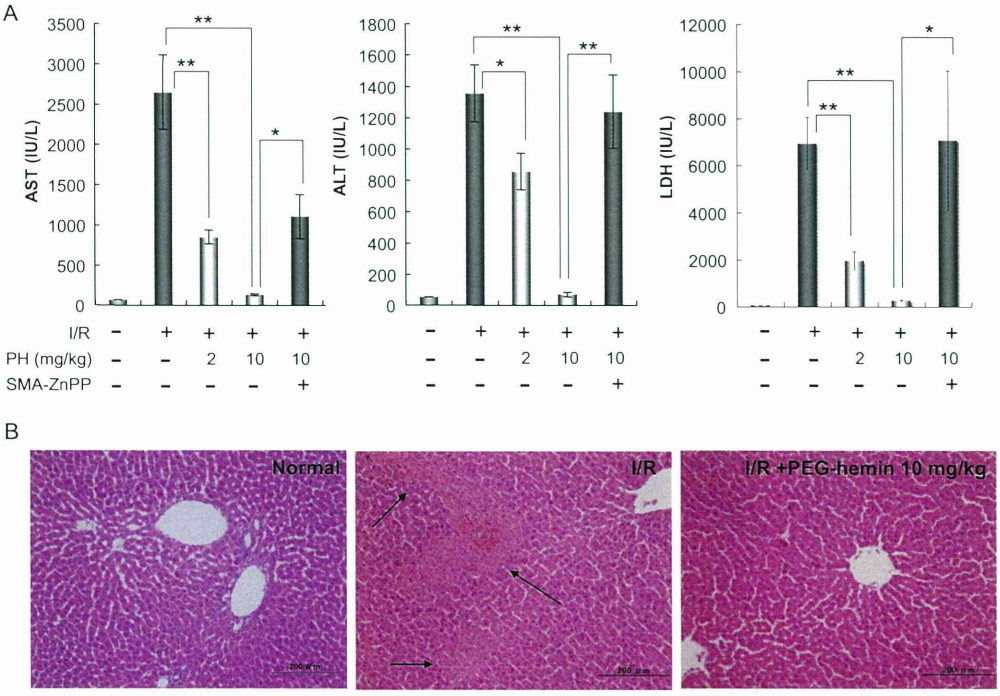

Fig. 6. Effect of PEG-hemin on hepatic I/R injury evaluated by changes in serum levels of AST, ALT, and LDH (A) and histological examination of rat liver tissue (B). Ischemia was induced by occluding both the portal vein and hepatic artery for 30 min followed by reperfusion for 3 h. PEG-hemin (PH) was administered intravenously 2 h before ischemia. The concentration of SMA-ZnPP administered to rats was 5 mg/kg. See *Amelioration of Liver I/R Injury by PEG-Hemin* under *Results* for details. Data are presented as means ± S.E. (n = 3–12). *, $P < 0.05$; **, $P < 0.01$. Arrows in B indicate necrotic areas of liver tissue.

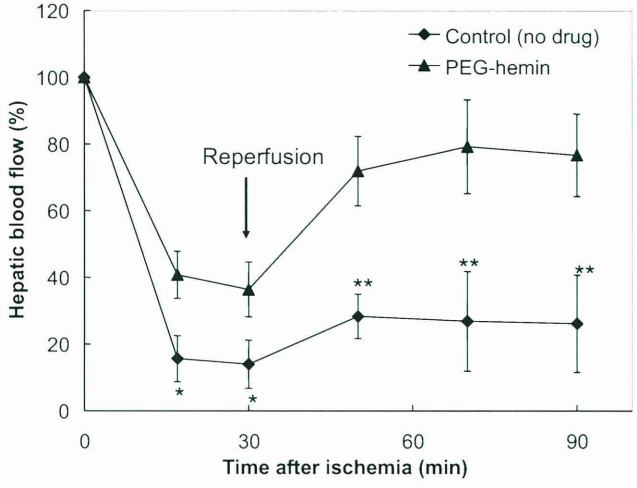

Fig. 7. Time profile of changes in hepatic blood flow before and after I/R and PEG-hemin treatment. Blood flow values are expressed as a percentage of the value measured before ischemia. PEG-hemin (10 mg/kg) was injected intravenously as noted in Fig. 6. Data are presented as means ± S.E. (n = 3–4). *, $P < 0.05$; **, $P < 0.01$, PEG-hemin versus native hemin.

(larger than 40 kDa) are known to have various beneficial characteristics including prolonged in vivo $t_{1/2}$ as shown above, and, what is more important, selective accumulation and retention in solid tumor and inflammatory tissues. This unique phenomenon of macromolecules was named the enhanced permeability and retention (EPR) effect (Matsumura and Maeda, 1986; Maeda et al., 2000, 2001; Duncan, 2003; Fang et al., 2011). Many macromolecular drugs have been developed on the basis of the EPR effect and are now not only at the laboratory stage of development but also in the clinical stage (Maeda et al., 2001; Duncan, 2003; Nagamitsu et al., 2009; Maeda, 2010; Fang et al., 2011).

In addition, the macromolecular PEG-hemin micelles showed relatively strong HO-1 induction activity, both in vitro and in vivo, as evidenced by mRNA and protein levels (Figs. 4B and 5A). More important was HO-1 enzymatic activity of generation of both antioxidative bilirubin and CO (Fig. 5, B and C), which are the essential components to exhibit the pharmacological effect of HO-1. By quantifying bilirubin production, one can assess the enzyme activity of HO. However, it may not reflect the physiological role of HO in vivo. Measurement of CO that is derived mostly from HO in biological organisms (Abraham and Kappas, 2008), in circulation, or tissues may thus useful to evaluate the physiological role of HO in vivo. The results presented in this study clearly indicated the correlation of the circulation CO level in parallel with HO expression and bilirubin production (Fig. 5). Further investigations are warranted for the measurement of CO levels in tissues.

Mechanisms involved in the tissue-protective and therapeutic effects of PEG-hemin were thought to rely mostly on the antioxidative role of HO-1, which would take advantage of the enzyme reactions in heme catabolism (Fang et al., 2004; Abraham and Kappas, 2008). Heme and free iron are pro-oxidants that would induce or enhance ROS generation (Akaike et al., 1992; Jeney et al., 2002), whereas bilirubin, which is a major product of heme degradation, is one of the most abundant endogenous antioxidants in mammals and accounts for the major antioxidative activity in human serum (Baranano et al., 2002).

More recently, CO generated during heme degradation is also believed to account for the major, if not all, biological properties of HO-1. HO-catalyzed heme catabolism is the major source of CO (i.e., more than 80%) in the mammalian system, and the roles of CO include, similarly to NO, regulating vascular tone (vasorelaxant), participating in antiapoptosis, serving an antioxidative, anti-inflammatory function, and inhibiting the activation of monocyte/macrophages, inducing angiogenesis, and others (Abraham and Kappas, 2008). In our present experiment, we found the CO concentration in circulation increased after PEG-hemin treatment (Fig. 5C), which was paralleled with the improved hepatic

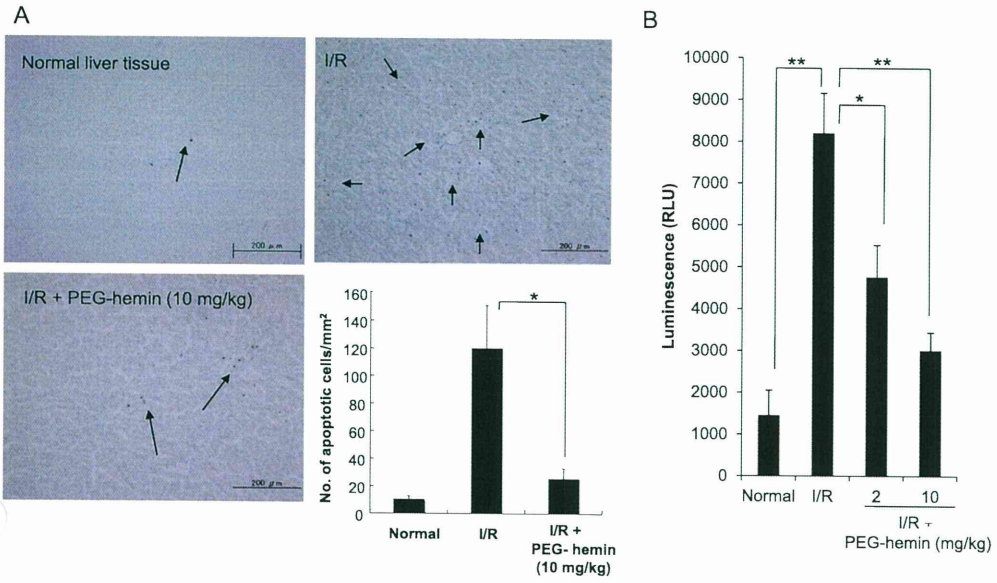

Fig. 8. Effect of PEG-hemin on I/R-induced apoptotic changes in the liver. Rats were treated with PEG-hemin before I/R, as given in Fig. 6. A, at 3 h after reperfusion, liver tissues were collected and paraffin-embedded sections were prepared for TUNEL staining (A). Arrows point to apoptotic cells. B, the caspase 3/7 activities in the liver tissues were also quantified. Data are presented as means ± S.E. (n = 3–6). *, $P < 0.05$; **, $P < 0.01$.

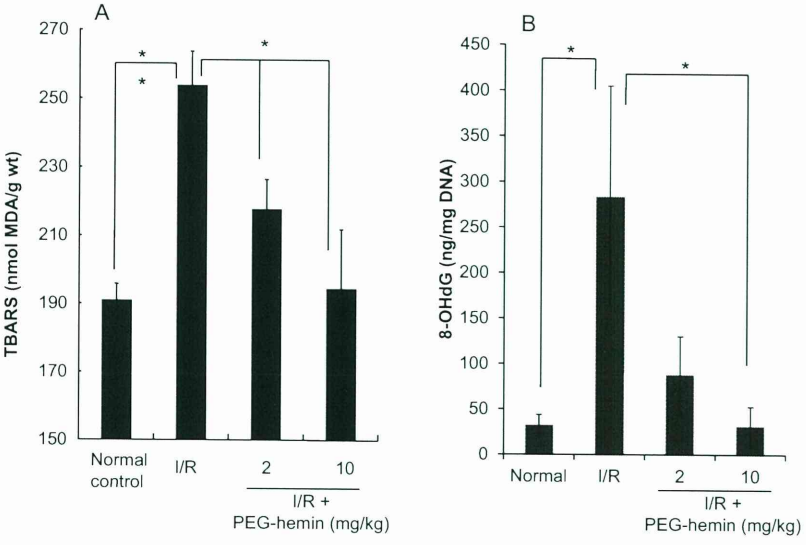

Fig. 9. TBARS (A) and 8-OHdG (B) in the rat liver after I/R injury with or without PEG-hemin treatment. The experimental protocol is the same as that noted in Fig. 6. At 3 h after reperfusion, rats were killed and the liver tissues were collected and subjected to the TBARS assay and ELISA of 8-OHdG (see *Materials and Methods* for details). Data are presented as means ± S.E. (n = 3–4). *, $P < 0.05$.

blood flow (Fig. 7) and decreased apoptosis in the liver in the I/R process (Fig. 8), even though we did not show direct evidence of its role on the cytoprotective effect against I/R injury. However, a recent study by Wei et al. (2010) demonstrated a direct effect of CO on I/R injury by using a CO-releasing molecule, although the effect was less significant, probably because of the short in vivo $t_{1/2}$ of CO-releasing agent.

In addition to HO-1 (the inducible enzyme), the constitutive form of HO, namely HO-2 is a major source of HO activity in most tissues. Both are alike in terms of enzymatic mechanisms of heme degradation and cofactor and substrate specificity (Maines, 1988; Abraham and Kappas, 2008). The HO activities in liver tissues measured in this study (Fig. 5B) may thus include HO-2 activity as well. Unlike HO-1, whose expression is relatively low in most normal tissues unless exposed to various stresses, such as I/R injury and hemin treatment as shown in this study (Fig. 5), HO-2 displays, in general, a constitutive expression in many normal tissues but it is not up-regulated upon stress or injury, which was also confirmed in this study (Supplemental Fig. 1). HO-2 is thus believed to contribute to normal housekeeping. And it has been reported that HO-2 behaves as a basal tone of anti-inflammatory signals, and deletion of HO-2 disables execution of the acute inflammatory and reparative response, leading to an exaggerated inflammatory response including increased oxidative stress and angiogenesis (Seta et al., 2006; Bellner et al., 2009). Moreover, it is known that HO-2 is induced by the treatment of corticosteroids (Maines et al., 1996), which is an important protective response during acute illness or stress, and is widely used as a treatment of inflammatory diseases. Thus, HO-2, along with HO-1, may also play important role as a protective response against I/R and inflammatory distress, facilitating the therapeutic response induced by PEG-hemin, which warranted further investigations.

I/R injury is a typical ROS-related inflammatory disorder, in which O_2^-, as a highly reactive radical, reacts with and oxidizes many biological molecules including NO (McCord, 1985; Maeda and Akaike, 1991; Ikebe et al., 2000) and thereby can trigger cell death. These pathological roles were clearly demonstrated in the present study using the I/R procedure, as evidenced by increased levels of the inflammatory cytokine MCP-1 (Fig. 10), elevated TBARS and 8-OHdG (Fig.

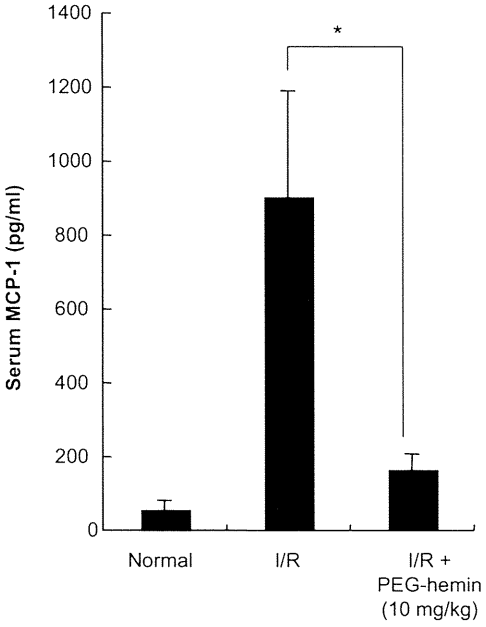

Fig. 10. Induction of MCP-1 by I/R injury and the protective effect of PEG-hemin. I/R and treatment protocols were the same as mentioned in Fig. 6. The serum MCP-1 concentration was measured by using an ELISA kit. Data are presented as means ± S.E. (n = 4–6). *, $P < 0.05$.

9), and apoptosis in liver tissue (Fig. 8), all of which were at least partly ameliorated by PEG-hemin treatment. As described above, O_2^- reacts extremely rapidly with NO at diffusion rate-dependent manner, and NO is thus removed and bioavailability of NO is reduced in the body, resulting in vascular constriction. These events explain, at least partly if not completely, the low hepatic blood flow after reperfusion during I/R, as Fig. 7 shows. Scavenging O_2^- will result in the reduction of apoptosis of hepatic cells and improve hepatic blood flow (Figs. 7 and 8). As a consequence, pathological effects caused by I/R injury will be prevented.

With regard to the treatment protocol in the present study, PEG-hemin was administered 2 h before ischemia was initiated, so as to achieve sufficient HO-1 induction, as shown in Fig. 5. This study used an acute I/R injury model, in which the injury peaked within 3 h, so that induction of HO-1 before I/R was necessary. Late treatment may be less effective because pathological changes progress quickly and may not be reversed before sufficient HO-1 expression. Acute I/R injury can in fact be observed in many medical interventions, such as routine operations, and especially organ transplantation, in which temporary obstruction of the blood flow of an organ or tissue is necessary, and the I/R injury of the tissue or organ is unavoidable and predictable. In these cases, prior administration of PEG-hemin and induction of HO-1 would be reasonable and practical and may produce successful therapeutic results. However, many I/R injuries seen in clinical settings are subacute or chronic, in which ROS are generated and injury progresses slowly but gradually; these situations include cardiac arrest, cerebral ischemia, thrombosis, and stroke (McCord, 1985). PEG-hemin may thus be beneficial in these cases with its long plasma half-life (Fig. 3; Table 1) and thus potent and sustained HO-1 induction activity. For groups at high risk of developing these diseases, PEG-hemin may become more important as a preventive medication because PEG-hemin itself demonstrated no or very little toxicity (Fig. 4A).

In addition, many disorders other than I/R injury are associated with ROS including inflammation, hypertension, and bacterial and viral infections (Maeda and Akaike, 1991; McCord, 2000). Therefore PEG-hemin may be applicable for the treatment of these diseases as well.

In conclusion, findings from the present study demonstrated that the macromolecular, water-soluble, micellar form of HO-1 inducer PEG-hemin exerted a potent cytoprotective effect against I/R injury of the liver in rats, as evidenced by low serum liver enzyme values (Fig. 6A), decreased numbers of apoptotic cells in the liver (Fig. 8), increased hepatic blood flow (Fig. 7), and reduced inflammatory cytokine levels in serum (Fig. 10). The cytoprotective effects of PEG-hemin can be attributed to augmented HO-1 activity (e.g., increased CO production, as Fig. 5C showed) through its antiapoptotic, antioxidative actions, because the HO-1 inhibitor SMA-ZnPP almost completely nullified the effect of PEG-hemin (Fig. 6A). This finding was also supported by the increased HO-1 mRNA and protein expression and elevated CO levels in blood and HO-1 enzyme activity (Figs. 4B and 5) and reduced tissue peroxidation in the liver after PEG-hemin treatment (Fig. 9). Therefore, the data presented herein suggest a therapeutic potential of PEG-hemin for I/R injury, and other ROS-related diseases, such as inflammatory disorders and hypertension, so PEG-hemin warrants further investigation as a therapeutic agent.

Acknowledgments

We thank Judith Gandy for editing the manuscript and Gahininath Y. Bharate for his excellent technical assistance.

Authorship Contributions

Participated in research design: Fang and Maeda.

Conducted experiments: Fang, Qin, Seki, Nakamura, and Tsukigawa.

Wrote or contributed to the writing of the manuscript: Fang, Qin, Shin, and Maeda.

References

Abraham NG and Kappas A (2008) Pharmacological and clinical aspects of heme oxygenase. *Pharmacol Rev* **60:**79–127.

Akaike T and Maeda H (2000) Pathophysiological effects of high-output production of nitric oxide, in *Nitric Oxide: Biology and Pathology* (Ignarro LJ ed) pp 733–745, Academic Press, San Diego.

Akaike T, Sato K, Ijiri S, Miyamoto Y, Kohno M, Ando M, and Maeda H (1992) Bactericidal activity of alkyl peroxyl radicals generated by heme-iron-catalyzed decomposition of organic peroxides. *Arch Biochem Biophys* **294:**55–63.

Baranano DE, Rao M, Ferris CD, and Snyder SH (2002) Biliverdin reductase: a major physiologic cytoprotectant. *Proc Natl Acad Sci U S A* **99:**16093–16098.

Beckman JS and Koppenol WH (1996) Nitric oxide, superoxide, and peroxynitrite: the good, the bad, and ugly. *Am J Physiol Cell Physiol* **271:**C1424–C1437.

Beckman KB and Ames BN (1997) Oxidative decay of DNA. *J Biol Chem* **272:**19633–19636.

Bellner L, Martinelli L, Halilovic A, Patil K, Puri N, Dunn MW, Regan RF, and Schwartzman ML (2009) Heme oxygenase-2 deletion causes endothelial cell activation marked by oxidative stress, inflammation, and angiogenesis. *J Pharmacol Exp Ther* **331:**925–932.

Berlett BS and Stadtman ER (1997) Protein oxidation in aging, disease, and oxidative stress. *J Biol Chem* **272:**20313–20316.

Davies KJ (1995) Oxidative stress: the paradox of aerobic life. *Biochem Soc Symp* **61:**1–31.

Doi K, Akaike T, Fujii S, Tanaka S, Ikebe N, Beppu T, Shibahara S, Ogawa M, and Maeda H (1999) Induction of haem oxygenase-1 nitric oxide and ischaemia in experimental solid tumours and implications for tumour growth. *Br J Cancer* **80:**1945–1954.

Duncan R (2003) The dawning era of polymer therapeutics. *Nat Rev Drug Discov* **2:**347–360.

Fang J, Akaike T, and Maeda H (2004) Antiapoptotic role of heme oxygenase (HO) and the potential of HO as a target in anticancer treatment. *Apoptosis* **9:**27–35.

Fang J, Iyer AK, Seki T, Nakamura H, Greish K, and Maeda H (2009a) SMA-

copolymer conjugate of AHPP: a polymeric inhibitor of xanthine oxidase with potential antihypertensive effect. *J Control Release* **135:**211–217.
Fang J, Nakamura H, and Maeda H (2011) The EPR effect: Unique features of tumor blood vessels for drug delivery, factors involved, and limitations and augmentation of the effect. *Adv Drug Deliv Rev* **63:**136–151.
Fang J, Sawa T, Akaike T, Akuta T, Sahoo SK, Khaled G, Hamada A, and Maeda H (2003) In vivo antitumor activity of pegylated zinc protoporphyrin: targeted inhibition of heme oxygenase in solid tumor. *Cancer Res* **63:**3567–3574.
Fang J, Seki T, and Maeda H (2009b) Therapeutic strategies by modulating oxygen stress in cancer and inflammation. *Adv Drug Deliv Rev* **61:**290–302.
Fang J, Seki T, Qin H, Bharate GY, Iyer AK, and Maeda H (2010) Tissue protective effect of xanthine oxidase inhibitor, polymer conjugate of (styrene-maleic acid copolymer) and (4-amino-6-hydroxypyrazolo[3,4-*d*]pyrimidine), on hepatic ischemia-reperfusion injury. *Exp Biol Med (Maywood)* **235:**487–496.
Halliwell B and Gutteridge JM (1984) Free radicals, lipid peroxidation, and cell damage. *Lancet* **2:**1095.
Ikebe N, Akaike T, Miyamoto Y, Hayashida K, Yoshitake J, Ogawa M, and Maeda H (2000) Protective effect of *S*-nitrosylated α_1-protease inhibitor on hepatic ischemia-reperfusion injury. *J Pharmacol Exp Ther* **295:**904–911.
Iyer AK, Greish K, Fang J, Murakami R, and Maeda H (2007) High-loading nanosized micelles of copoly(styrene-maleic acid)-zinc protoporphyrin for targeted delivery of a potent heme oxygenase inhibitor. *Biomaterials* **28:**1871–1881.
Jeney V, Balla J, Yachie A, Varga Z, Vercellotti GM, Eaton JW, and Balla G (2002) Pro-oxidant and cytotoxic effects of circulating heme. *Blood* **100:**879–887.
Maeda H (2010) Tumor-selective delivery of macromolecular drugs via the EPR effect: background and future prospects. *Bioconjug Chem* **21:**797–802.
Maeda H and Akaike T (1991) Oxygen free radicals as pathogenic molecules in viral diseases. *Proc Soc Exp Biol Med* **198:**721–727.
Maeda H, Sawa T, and Konno T (2001) Mechanism of tumor-targeted delivery of macromolecular drugs, including the EPR effect in solid tumor and clinical overview of the prototype polymeric drug SMANCS. *J Control Release* **74:**47–61.
Maeda H, Wu J, Sawa T, Matsumura Y, and Hori K (2000) Tumor vascular permeability and the EPR effect in macromolecular therapeutics: a review. *J Control Release* **65:**271–284.
Maines MD (1988) Heme oxygenase: function, multiplicity, regulatory mechanisms, and clinical applications. *FASEB J* **2:**2557–2568.
Maines MD, Eke BC, and Zhao X (1996) Corticosterone promotes increased heme oxygenase-2 protein and transcript expression in the newborn rat brain. *Brain Res* **722:**83–94.
Matsumura Y and Maeda H (1986) A new concept for macromolecular therapeutics in cancer chemotherapy: mechanism of tumoritropic accumulation of proteins and the antitumor agent smancs. *Cancer Res* **46:**6387–6392.
McCord JM (1985) Oxygen-derived free radicals in postischemic tissue injury. *N Engl J Med* **312:**159–163.
McCord JM (2000) The evolution of free radicals and oxidative stress. *Am J Med* **108:**652–659.
Melgarejo E, Medina MA, Sánchez-Jiménez F, and Urdiales JL (2009) Monocyte chemoattractant protein-1: a key mediator in inflammatory processes. *Int J Biochem Cell Biol* **41:**998–1001.
Miyamoto Y, Akaike T, Yoshida M, Goto S, Horie H, and Maeda H (1996) Potentiation of nitric oxide-mediated vasorelaxation by xanthine oxidase inhibitors. *Proc Soc Exp Biol Med* **211:**366–373.
Muzykantov VR, Atochina EN, Ischiropoulos H, Danilov SM, and Fisher AB (1996) Immunotargeting of antioxidant enzyme to the pulmonary endothelium. *Proc Natl Acad Sci U S A* **93:**5213–5218.
Nagamitsu A, Greish K, and Maeda H (2009) Elevating blood pressure as a strategy to increase tumor-targeted delivery of macromolecular drug SMANCS: cases of advanced solid tumors. *Jpn J Clin Oncol* **39:**756–766.
Oda T, Akaike T, Hamamoto T, Suzuki F, Hirano T, and Maeda H (1989) Oxygen radicals in influenza-induced pathogenesis and treatment with pyran polymer-conjugated SOD. *Science* **244:**974–976.
Ohkawa H, Ohishi N, and Yagi K (1979) Assay for lipid peroxides in animal tissues by thiobarbituric acid reaction. *Anal Biochem* **95:**351–358.
Roy RS and McCord JM (1983) Superoxide and ischemia: conversion of xanthine dehydrogenase to xanthine oxidase, in *Oxyradicals and Their Scavenger Systems* (Greenwald R, and Cohen G eds) pp 145–153, Elsevier Science, New York.
Sahoo SK, Sawa T, Fang J, Tanaka S, Miyamoto Y, Akaike T, and Maeda H (2002) Pegylated zinc protoporphyrin: a water-soluble heme oxygenase inhibitor with tumor-targeting capacity. *Bioconjug Chem* **13:**1031–1038.
Sawa T, Wu J, Akaike T, and Maeda H (2000) Tumor-targeting chemotherapy by a xanthine oxidase-polymer conjugate that generates oxygen-free radicals in tumor tissue. *Cancer Res* **60:**666–671.
Seta F, Bellner L, Rezzani R, Regan RF, Dunn MW, Abraham NG, Gronert K, and Laniado-Schwartzman M (2006) Heme oxygenase-2 is a critical determinant for execution of an acute inflammatory and reparative response. *Am J Pathol* **169:**1612–1623.
Stocks SJ, Jones AJ, Ramey CW, and Brooks DE (1986) A fluorometric assay of the degree of modification of protein primary amines with polyethylene glycol. *Anal Biochem* **154:**232–234.
Wei Y, Chen P, de Bruyn M, Zhang W, Bremer E, and Helfrich W (2010) Carbon monoxide-releasing molecule-2 (CORM-2) attenuates acute hepatic ischemia reperfusion injury in rats. *BMC Gastroenterol* **10:**42.

Address correspondence to: Professor Hiroshi Maeda, DDS Research Institute, Sojo University, Kumamoto 860-0082, Japan. E-mail: hirmaeda@ph.sojo-u.ac.jp

Current Cancer Drug Targets, 12(1), 51-63 (2012)

The Hsp32 inhibitors SMA-ZnPP and PEG-ZnPP exert major growth-inhibitory effects on $CD34^+/CD38^+$ and $CD34^+/CD38^-$ AML progenitor cells

Harald Herrmann[1,2], Michael Kneidinger[2], Sabine Cerny-Reiterer[2], Thomas Rülicke[3], Michael Willmann[4], Karoline V. Gleixner[2], Katharina Blatt[2], Gregor Hörmann[5], Barbara Peter[2,4], Puchit Samorapoompichit[6], Winfried Pickl[7], Gahininath Yadavrao Bharate[8], Matthias Mayerhofer[5], Wolfgang R. Sperr[2], Hiroshi Maeda[8], Peter Valent[1,2]*

[1]Ludwig-Boltzmann Cluster Oncology, Vienna, Austria; [2]Department of Internal Medicine I, Division of Hematology & Hemostaseology, Medical University of Vienna, Austria; [3]Institute of Laboratory Animal Science, University of Veterinary Medicine Vienna, Austria; [4]Department of Companion Animals and Horses, Clinic for Internal Medicine and Infectious Diseases, University of Veterinary Medicine Vienna, Austria; [5]Department of Laboratory Medicine, [6]Center of Anatomy and Cell Biology & [7]Institute of Immunology, Medical University of Vienna, Austria; [8]Laboratory of Microbiology and Oncology, Faculty of Pharmaceutical Sciences, Sojo University, Kumamoto and BioDynamics Research Laboratory, Kumamoto, Japan

Supported by: Austrian Federal Ministry for Science and Research (GENAU-C.h.i.l.d. grant #GZ 200.136/1-VI/1/2005), a Cancer Stem Cell grant and Initative Krebsforschung of the Medical University of Vienna; and a grant for Cancer Research from the Ministry of Education, Science, Culture, and Sports of Japan (#17016076).

Running Title: Effects of HO-1-blockers on AML cells

*Correspondence:
Peter Valent, MD
Department of Internal Medicine I
Division of Hematology & Hemostaseology
Medical University of Vienna
Ludwig Boltzmann Cluster Oncology
AKH-Wien, Währinger Gürtel 18-20
A-1097 Vienna, Austria
Phone: +43-1-40400-4416; Fax: +43-1-40400-4030
E-mail: peter.valent@meduniwien.ac.at

Abstract word count: 224 Total word count: 5,558

Key words: AML • HO-1 • Hsp32 • survival • targeting

ABSTRACT

Heat shock protein 32 (Hsp32), also known as heme oxygenase 1 (HO-1), has recently been identified as a potential target in various hematologic malignancies. We provide evidence that Hsp32 is constitutively expressed in primary leukemic cells in patients with acute myeloid leukemia (AML) and in various AML cell lines (HL60, U937, KG1). Expression of Hsp32 mRNA was demonstrable by qPCR, and expression of the Hsp32 protein by immunocytochemistry and Western blotting. The stem cell-enriched CD34+/CD38+ and CD34+/CD38- fractions of AML cells were found to express Hsp32 mRNA in excess over normal CD34+ progenitor cells. Two Hsp32-targeting drugs, pegylated zinc-protoporphyrin (PEG-ZnPP) and styrene-maleic-acid-copolymer-micelle-encapsulated ZnPP (SMA-ZnPP), were found to inhibit cytokine-dependent and spontaneous proliferation in all 3 AML cell lines as well as in primary AML cells. Growth inhibitory effects of SMA-ZnPP and PEG-ZnPP were dose-dependent with IC_{50} values ranging between 1 and 20 μM, and were accompanied by apoptosis as evidenced by light- and electron microscopy, Tunel assay, and caspase-3 activation. Finally, we were able to demonstrate that SMA-ZnPP inhibits cytokine-dependent proliferation of CD34+/CD38+ and CD34+/CD38- AML progenitor cells *in vitro* in all patients as well as leukemia-initiation of AML stem cells in NOD-SCID IL-2R$\gamma^{-/-}$ (NSG) mice *in vivo*. Together, our data suggest that Hsp32 plays an important role as a survival factor in leukemic stem cells and as a potential new target in AML.

Introduction

Acute myeloid leukemia (AML) is a life-threatening neoplasm characterized by uncontrolled proliferation and accumulation of myeloblasts in hematopoietic tissues [1,2]. Clinical features and the prognosis in AML vary depending on deregulated genes, the cell type(s) involved, and the biological properties of the clone [1-4]. In a group of patients, cytogenetic features are indicative of a favorable prognosis [1,2,5]. These patients, when treated with repeated cycles of chemotherapy or hematopoietic stem cell transplantation (HSCT), have a relatively high chance to enter long-term disease-free survival [5-8]. However, not all patients have a suitable donor or are eligible for HSCT. In other patients, the response to chemotherapy is poor or short-lived. For AML patients who cannot be cured by chemotherapy or HSCT, no effective treatment alternatives are available and the prognosis is grave.

During the past few years, a number of new promising targeted drugs have been developed in clinical hematology [9-11]. A highlighting example is chronic myeloid leukemia (CML) where drugs targeting the disease-related oncoprotein, BCR/ABL, produce complete cytogenetic remission in a majority of all patients [11,12]. In AML, however, targeted drugs with comparable beneficial effects have not been developed yet. This may be due to the heterogeneity of the disease and the fact that many different oncogenes, downstream signaling pathways, and survival molecules play a role in disease evolution [3,4,9,10]. Therefore, in AML, research is currently attempting to identify not only disease-specific targets but also targets that are broadly expressed in leukemic cells in various categories of the disease [9,10,13].

One interesting group of targets in hematology are heat shock proteins (Hsp) [14-16]. These stress-related proteins act cytoprotective and anti-apoptotic in neoplastic cells in various (myeloid) leukemias [14-16]. However, so far, little is known about the expression and role of various Hsp in AML, and the effects of Hsp-targeting drugs. A particular problem is that only a few Hsp-targeting drugs are available.
Hsp32, also known as heme oxygenase-1 (HO-1), is an inducible stress-protein that acts anti-apoptotic and cytoprotective in various cells in inflammatory reactions [17,18]. More recently, it has been described that Hsp32 is also employed as a survival factor by neoplastic cells and may serve as an interesting target [19-24]. We have recently shown that leukemic cells in CML express Hsp32 in a constitutive manner, and that Hsp32 may represent a potential target in CML [25,26].
The aims of the present study were to examine the expression and functional role of Hsp32 in AML cells and to explore whether targeting of Hsp32 in leukemic (progenitor) cells is associated with apoptosis and growth arrest.

MATERIALS AND METHODS

Reagents

RPMI 1640 medium and fetal calf serum (FCS) were purchased from PAA laboratories (Pasching, Austria), hemin, cytosine arabinoside (ARA-C), and zinc-protoporphyrin (ZnPP) from Sigma-Aldrich (St. Louis, MO), and ^{3}H-thymidine from Amersham (Aylesbury, UK). Recombinant human (rh) granulocyte-macrophage colony-stimulating factor (GM-CSF) was provided by Sandoz (Vienna, Austria) and rh interleukin-3 (IL-3) by Novartis (Vienna, Austria). Rh stem cell factor (SCF) was purchased from PeproTech (Rocky Hill, NJ), and rh G-CSF from Amgen (Thousand Oaks, CA). Pegylated zinc protoporphyrin (PEG-ZnPP) and styrene maleic acid-copolymer-encapsulated zinc protoporphyrin (SMA-ZnPP) were produced at Sojo University (Kumamoto, Japan) as described [23,24,27]. The following monoclonal antibodies (mAb) were used in our flow cytometry experiments: the FITC-conjugated CD19 mAb 4G7, PE-labeled CD33 mAb WM53, PE- or FITC-conjugated CD34 mAb 581, APC-labeled CD38 mAb HIT2, and the PerCP-labeled CD45 mAb 2D1 (all from Becton Dickinson Biosciences, San Jose, CA).

Isolation of primary AML cells and culture of cell lines

Primary leukemic cells were obtained from the peripheral blood (PB) or/and bone marrow (BM) of 58 patients with either untreated AML (de novo or secondary) or relapsed/refractory AML before therapy. Diagnoses were established according to published criteria [2,28,29]. The patients´ characteristics are shown in Table 1. Detailed information on all patients including the French-American-British (FAB) cooperative study group subtype and the WHO subtype of AML are provided in supplemental Table S1. Informed consent was obtained prior to blood donation and BM puncture in each case. Mononuclear cells (MNC) were isolated using Ficoll. In a separate set of experiments, cells were preincubated with hemin (10 μM) or control medium at 37°C for 4 hours before being analyzed for Hsp32 expression [25]. In 12 patients, CD34+/CD38+ and CD34+/CD38- cells were purified to homogeneity by mAb and cell sorting on a FACSAria (Becton Dickinson Biosciences) following

published techniques [30,31]. The purity of sorted cells amounted to >98%. The following AML cell lines were used: HL60, U937, and KG1. Cell lines were obtained from the DSMZ Institute (Braunschweig, Germany) and maintained in RPMI 1640 medium with 10% FCS at 37°C.

^{3}H-thymidine incorporation assay

Unfractionated AML cells (MNC), sorted CD34+/CD38- and CD34+/CD38+ AML cells, and cell lines were cultured in 96-well microtiter plates (1-5 x 10^4 cells/well) in the absence or presence of PEG-ZnPP or SMA-ZnPP (100 nM to 50 μM) at 37°C for up to 48 hours. Unfractionated MNC were kept with or without GM-CSF (100 ng/ml). Proliferation of sorted AML progenitor cells was induced by a cytokine-cocktail containing SCF (100 ng/ml), IL-3 (100 ng/ml), GM-CSF (100 ng/ml), and G-CSF (100 ng/ml). After exposure to drugs, 0.5 μCi ^{3}H-thymidine was added (12 hours). Cells were then harvested on filter membranes in a Filtermate 196 harvester (Packard Bioscience, Meriden, CT). Filters were air-dried, and the bound radioactivity was measured in a β-counter (Top-Count NXT, Packard Bioscience). In a separate set of experiments, AML cell lines were incubated with various concentrations of ZnPP (0.1-10 μM) or with combinations of Hsp-32-targeting drugs and ARA-C at a fixed dose-ratio (48 hours). All experiments were performed in triplicates.

Immunocytochemistry

Immunocytochemistry was performed on cytospin-slides prepared from primary leukemic cells (BM or PB MNC from 43 patients) as reported [25] using a polyclonal rabbit anti-HO-1 antibody. Newfuchsin (Nichirei, Tokyo, Japan) was used as chromogen. In control experiments, the primary antibody was omitted, was pre-incubated with control buffer, or was preincubated with a HO-1-specific blocking peptide (Stressgen Biotechnologies, Victoria, BC, Canada) prior to staining.

Quantitative PCR (qPCR)

PCR experiments were performed on RNA from unfractionated MNC as well as sorted CD34+/CD38+ and CD34+/CD38- cells (AML, n=10, cord blood cells pooled from 3 donors). mRNA levels were quantified on a 7900HT Fast Real-Time PCR System from Applied Biosystems (Foster City, CA), using iTaq SYBR Green Supermix with ROX from Bio-Rad (Hercules, CA) and Abl as reference gene as reported [26,32]. In addition, conventional PCR was performed. Primers used are shown in Table 2. In a separate set of experiments, unfractionated AML cells (n=6 donors) were exposed to control medium or hemin (10 μM) at 37°C for 4 hours prior to RNA isolation and qPCR analysis. Stable HO-1 knock-down in U937 cells was generated by transduction with a microRNA (miRNA) adapted retroviral vector as described [33]. Briefly, the LMP-miHO1 vector was used to produce recombinant VSV-G pseudotyped retroviruses. Cells were transduced in the presence of polybrene (7 μg/mL) and GFP positve cells were sorted on a FACSAria (Becton Dickinson Biosciences). Knock-down of HO-1 was confirmed by Western blotting.

Preparation of cell lysates and Western blotting

Western blot experiments were performed on primary AML cells and AML cell lines as described [25]. Cell lines were incubated in control medium with or without hemin

(10 μM) at 37°C for 4 hours. After washing cells, protein-fractions were separated by SDS-polyacrylamide gel-electrophoresis and transferred to nitrocellulose membranes. For detection of Hsp32, a rabbit polyclonal anti-HO-1 antibody (Stressgen) and goat anti-rabbit IgG (Amersham) were applied. To confirm equal loading, membranes were re-probed with a rabbit anti-ß-actin antibody (Sigma-Aldrich).

Evaluation of apoptosis by microscopy and Tunel assay

Primary AML cells and cell lines were incubated with PEG-ZnPP or SMA-ZnPP (each 1–20 μM) at 37°C for up to 48 hours. In a separate set of experiments, leukemic cells were incubated with various concentrations of ZnPP (1-50 μM) for up to 48 hours. Apoptotic cells were identified as reported [34] and quantified on Wright-Giemsa-stained cytospin preparations. In select experiments, the pan-caspase-inhibitor Z-VAD-FMK (50 μM) (Enzo Life Sciences, Farmingdale, NY, USA) was added for 24 hours to AML cell lines exposed to SMA-ZnPP. To confirm apoptosis, electron microscopy was performed as reported [35] using U937 cells incubated with SMA-ZnPP (20 μM) or control medium for 48 hours. Sections were viewed under a JEOL 1200 EX II electron microscope (JEOL, Tokyo, Japan). Typical signs of apoptosis including nuclear fragmentation and chromatin condensation were recorded. To confirm apoptosis in drug-exposed cells, a Tunel assay was performed as reported [35]. In brief, AML cell lines were cultured in control medium, PEG-ZnPP (20 μM) or SMA-ZnPP (20 μM) at 37°C for 3 days. Thereafter, cells were recovered, fixed in 1% formaldehyde, treated with 70% ice-cold ethanol for 1 hour, washed, and incubated in terminal-transferase reaction-solution containing $CoCl_2$, DNA deoxy-nucleotidyl-exotransferase, and biotin-16-2´-deoxy-uridin-5´-triphosphate (Boehringer Mannheim, Germany) at 37°C for 10 minutes [35]. Then, cells were washed, incubated with Streptavidin Fluorescein, and analyzed with a Nikon Eclipse E 800 fluorescence microscope (Tokyo, Japan).

Detection of active caspase 3 by flow cytometry

AML cell lines were incubated in control medium or various concentrations of SMA-ZnPP or PEG-ZnPP at 37°C for 48 hours. Then, cells were fixed in 2% formaldehyde for 10 minutes, permeabilized in 100% methanol at -20°C (15 minutes), washed in PBS plus BSA (0.1%), then stained with FITC-conjugated mAb C92-605 (Becton Dickinson Biosciences) directed against active caspase 3 (1 hour), and then analyzed by flow cytometry on a FACSCalibur (Becton Dickinson Biosciences). In select experiments, cell cycle distribution in drug-exposed AML cells was examined by flow cytometry after permeabilization of cells with 0.1% Triton X-100 and DNA-staining with propidium iodide (PI).

Repopulation of AML cells in NOD-SCID IL-2Rgamma^{null} (NSG) mice

Primary AML cells (n=3 experiments) were incubated in control medium or in SMA-ZnPP (20 μM) with 10% FCS at 37°C for 2 hours. After incubation, AML cells were fully viable cells without signs of apoptosis as assessed by trypan blue exclusion and Wright-Giemsa staining (not shown). Drug exposed cells were washed, resuspended in 0.15 ml PBS with 2% FCS, and injected into the tail vein of adult female NSG mice (2-5 x 10^6 per mouse, 4 mice per group) (The Jackson Laboratory, Bar Harbor, ME). Twenty four hours prior to injection, mice were irradiated (2.4 Gy). After injection,